Post-Breakup Lithosphere Recycling below the U.S. East Coast: Evidence From Adakitic Rocks

Romain Meyer, Centre for Geobiology & Department of Earth Science, University of Bergen, Bergen, Norway, mail@romain-meyer.eu

Jolante van Wijk, Department of Earth and Environmental Science, New Mexico Institute of Mining and Technology, Socorro, NM, USA, jvanwijk@nmt.edu

Abstract

We present here the first geochemical data of adakitic rocks from an extensional system - the U.S. East Coast rifted margin. Adakitic magmas are high-K melts that have petrogenetically been interpreted to be partial melts of subducting slab and/or lower crustal lithologies in delamination events. The adakitic rocks presented here are from a small volcanic region in the Valley and Ridge province in Virginia, and were probably emplaced around the time of continent rupture and Central Atlantic Magmatic Province activity. They are bi-modal in character (high-Si and low-Si), and have the typical high and low-Si adakitic geochemical characteristics such as high K_2O (up to 9.88 wt. %) abundances, steep REE patterns and significantly high Sr (2473 ppm), but relatively low Rb (35 ppm) contents (high-Si adakitic rocks). The petrogenetic relation of these melts to partial melting of metagabbroic rocks (high-Si adakites) and interaction of these melts with ambient peridotite (low-Si adakites) suggests that the geodynamic process for the formation of the studied Jurassic Central Virginia igneous rock succession is delamination of mantle lithosphere and lower crust below the volcanic rifted margin. We present with geodynamic models that negatively buoyant mantle lithosphere instabilities developed below this passive margin during continent rupture. After foundering, warm asthenosphere welled up and heated the lower crust of the East Coast margin, which was interspersed in our study area with fragmented hydrated metamorphic mafic to ultramafic lithologies. In-situ and/or dripping melting of such meta-igneous rocks reproduces the observed geochemistry of the studied high-Si adakitic rocks. Further recycling processes within the convecting mantle of delaminated floating fertile meta-igneous rock packages could be responsible for Atlantic melting anomalies such as the Azores or Bermuda.

Key words: Continental breakup, lithospheric instabilities, adakites, US E-coast margin

1. Introduction

Anderson (2005) speculated that formation of Large Igneous Provinces such as the Kerguelen Plateau might be due to recycled eclogite packages within the mantle. The gravitational removal of mafic lower crustal layers with lithospheric mantle over a large area results in upwelling of the underlying asthenosphere, which starts to melt partially due to decompression and fluid injections (e.g. Bird et al., 1979; Esedo et al., 2013). Significant volumes of magmatism are assumed to result from this process. Theoretically, magma is further produced when the delaminated crustal material is heated, dehydrated and recycled back into the mantle; it was subsolidus while emplaced within the continental lithosphere, but will start melting in the upper mantle (Elkins-Tanton, 2005). Such delamination or gravitational removal ("dripping") of lithosphere material can be simplistically explained as foundering of dense lithosphere into less dense asthenosphere. It results from lateral density variations in the lithosphere that form lithosphere-asthenosphere boundary instabilities (e.g., Bird, 1979; Houseman et al., 1981; Houseman and Molnar, 1997; King and Anderson, 1998; Conrad and Molnar, 1997; Dumoulin et al., 2005). Such lateral density variations can be inherited; for example the lithospheric layering in the North American Craton (Yuan and Romanowicz, 2010) results from magmatic intrusions forming dense cumulates. Instabilities may also develop when lateral variations in temperature and density form during continental rifting (Sleep, 2007). During sinking the lithospheric material will interact with the surrounding hotter asthenosphere by exchanging heat, fluids and melts, while the overlying crust deforms and moves vertically. In recent decades, such lithospheric instabilities have been invoked as an explanation for intra-plate magmatism, lithospheric deformation and increased melt production (e.g., Large Igneous Provinces: Kay and Mahlburg Kay, 1993; Elkins-Tanton, 2005; 2007; and, on a smaller scale, the Sierra Nevada drip- Zandt et al., 2004, Saleeby et al., 2003; 2012; 2013; Saleeby and Foster, 2004; and Colorado Plateau- van Wijk et al., 2010; Levander et al., 2011).

Following delamination of lower crust and mantle lithosphere, the upwelling mantle heats the overlying crust, and may cause anatexis of the crustal material. This process has been described for formation of adakitic igneous rocks in the Himalayas (e.g. Wang et al. 2005) and Andes (e.g. Atherton and Petford, 1993). Adakites are igneous rocks with geochemical similarities to synthetic melts from melting experiments of (meta-) basalt (e.g. Rapp and Watson, 1995). As a result, the petrogenesic source of adakites can be related to partial melting of metamorphic mafic lithologies; either from partial melting within subducting oceanic crust and/or by direct fusion of lower crustal lithologies. These processes have had far-reaching consequences for conceptual and geodynamic models; the first was a milestone in our understanding of the subduction factory, and the second model has the potential to cast not only light on interactions of a thickened lithosphere with the asthenosphere but also on Archean geodynamics. Here we report for the first time on adakites from the continental margin of the U.S. East coast that spatially and temporally relate to the Mesozoic opening of the North Atlantic. We relate the adakites to mantle lithosphere destabilization below the continental margin, a process that starts around the time of continental breakup.

Definition of adakites in this study

The term "adakite" was introduced by Defant and Drummond (1990) to describe Cenozoic volcanic arc volcanic and plutonic rocks. The melts are petrogenetically derived from melting of subducting hot and young basaltic oceanic crust. Later studies found that this slab melting process is not restricted to subduction factories

recycling young oceanic crust (e.g. Castillo, 2006). Geochemically the dacitic to andesitic rocks were initially defined by high SiO_2 (≥ 56 wt.%), Al_2O_3 (≥ 15 wt.%), and Sr (> 400 ppm) abundances, with low MgO concentrations (< 3wt.%), and high Sr/Y (> 20) and La/Yb (> 20) ratios. The characteristic geochemistry was explained as a partial melting product of an eclogitic or amphibolitic meta-basalt. This petrogenetic model has been supported by experimental petrology observations (e.g. Rapp and Watson, 1995), reproducing similar high-Si and high-K partial melts from meta-basalts.

Phaneritic trondheimites have similar geochemical signatures as adakites. This close compositional similarity between the adakites and the Archean tonalite-trondheime-granodiorite (TTG) suite has been interpreted to result from a similar process and geodynamic source (Martin, 1999). The similarities between recent subduction zone melts and TTGs can be used (e.g. Drummond and Defant, 1990) to gain insight into plate tectonic processes during the Archean (e.g. Hamilton, 1998, 2007, 2011; Stern, 2005, 2008). Smithies (2000) however, pointed out that the compositional similarity between TTG and adakites reflects only a similar partial melting source under similar conditions, which are not unique to subduction zones. Smithies (2000) preferred an in-situ melting model for the TTG series of lower crustal hydrous mafic material at the base of a thickened crust. He supported his interpretation by the fact that the Archean TTG geochemistry shows no or limited geochemical signatures for melt – peridotite interactions. This is in contrast to arc-related adakites, where anomalously high MgO, Ni, Cr and low SiO_2 concentrations are well known since Kay (1978) reported on high-MgO adakites from the Aleuten arc.

Low-Si high-MgO adakites are not in agreement with the above described original major element geochemical discriminants, and so the definition of adakites can only be based on trace element characteristics. Low-Si adakites are believed to result when "pure" high-Si adakite melts are interacting with ambient mantle peridotite (e.g. Kay, 1978; Smithies, 2000). Experimentally such melt – ultramafic rock interactions have been linked to fractional crystallization of garnet and orthopyroxene in the mantle lithology from the "pure" high-Si adakite (e.g. Yogodzinski, et al. 1995; Rapp et al., 1999). The initial andesitic high-Si adakite composition evolves in such experiments to alkalic melts through basanite and nephelinite (Mallik and Dasgupta, 2013; 2014). Based on rock interacting melt ratios Yaxley and Green (1998) showed that a majority of high-Si adakites (slab melts) would freeze in the mantle and so metasomatize the ambient peridotite. Low-Si adakites would then represent low degrees of decompression partial melting from a metasomatized peridotite mantle source. As both adakitic rock types are described in most arc localities (e.g. Castillo, 2006) as well as in this study, we use in this paper the term high-Si adakites for "pure" meta-basalt partial melts and low-Si adakites for "pure" high-Si adakitic melts having interacted with ambient peridotite.

2. CAMP magmatism during Atlantic breakup

The breakup of Pangaea not only resulted in continental fragmentation and the present continent-ocean distribution, but also produced extensive volcanism along the developing Atlantic margins. This excessive volcanic activity caused some of the largest known Large Igneous Provinces (LIPs); the Central Atlantic Magmatic Province (CAMP) (e.g. Marzoli et al., 1999), and the North Atlantic Igneous Province (NAIP) (e.g. Meyer et al., 2007). These LIPs are generally attributed to mantle plumes, edge-convection, or rifting above fertile mantle (Meyer et al., 2007, for an overview). During the breakup of Pangaea, continental margins were at shallow

marine depths, or above sea level. This could be the result of loss of mantle lithosphere below the continent margins, for example as a result of destabilization of subcontinental mantle (Sleep, 2007; Esedo et al., 2012).

Direct evidence for such destabilizations have yet to be found. The NAIP area was tectonically overprinting the Caledonian orogenesis when Jurassic extension began, and conditions for the development of a gravitationally unstable lithospheric root and consequential delamination were likely present in the North East Atlantic (Meyer et al., 2007). Meyer et al. (2007) found that delamination could not have caused the excessive NAIP volcanism, as the majority of available NAIP melt compositions are not in agreement with predicted characteristic high K, Al, and large ion lithophile element (LILE) compositions with high La/Yb, normally related to delamination (e.g. Kay and Mahlburg Kay, 1993; Smithies, 2000). However such high-potassium igneous rocks would only represent a small fraction of the integral LIP volcanic products if delamination occurred *after* breakup on a local instead of regional scale. In addition, sampling some of the world largest and partly offshore LIPs could be biased toward the most common melts.

Delamination in the southern Appalachian CAMP area has been linked to the Alleghanian orogeny (e.g. Nelson, 1992; Sacks and Secor, 1990). An Alleghanian delamination event might have had substantial control on the subsequent generation of basaltic magmas during Mesozoic rifting (Nelson, 1992), as the extension needed for rift-induced decompression melting was insufficient (Harry and Sawyer, 1992). The small magmatic province that is the focus of the present study is located within the CAMP. Its unusual geochemistry but spatial and potentially timely relation to the central Atlantic breakup casts light on intrinsic petrogenetic processes during lithospheric delamination in an extensional setting.

Common CAMP tholeiitic dykes and sills are spread over four continents surrounding the central Atlantic Ocean (Marzoli et al., 1999). Puffer (2003) reported that although several Mesozoic magma types are found within this area, peak magmatic activity is characterized by tholeiitic melts with a uniform composition (e.g. 1 wt.% TiO_2). The homogeneous main CAMP geochemistry is significantly different from typical N-MORB or OIB melts and shows little-to-no *in situ* crustal contamination (Puffer, 2003; Callegaro et al., 2013). Pegram (1990) postulated that the source of this CAMP signature would be the subcontinental lithospheric mantle (SCLM) overprinted and contaminated during the Greenville orogeny with an arc mantle. Based on geochemical trace element signatures Puffer (2003) readopted this idea while linking the CAMP melting source to the same mantle that produced the arc / back-arc melts during Pangea formation. These subduction signatures in the classical tholeiitic CAMP melts with the geographical correlation between the main igneous activity and plate sutures from Pangea closure all point toward an arc-like SCLM composition. Callegaro et al. (2013) explained the extremely low $^{206}Pb/^{204}Pb$ with high $^{207}Pb/^{204}Pb$ variations within the U.S. Southeastern CAMP tholeiites as a geographically restricted source of lower continental crustal material within the melting source. They suggest that during the Paleozoic subduction events lower continental crust was recycled locally into the shallow mantle. Merle et al. (2013) confirmed that the geochemical crust-like CAMP characteristics are neither the result from crustal contamination nor unusual isotopic compositions within a mantle plume. These authors favor a mantle-source for the CAMP, where crustal sediments were incorporated into the asthenospheric mantle wedge during Paleozoic subduction.

The present study does not focus on these dominant CAMP tholeiitic rocks, but on a small Jurassic high-K igneous rock succession in West Central Virginia (Figure 1).

We present a systematic whole rock major- and trace element study and develop a geodynamic model that may explain the location, timing and geochemistry of the rocks. The only published geochemical compositions from these uncommon rocks are 4 major element analyses by Watson and Cline (1913). Bulk geochemical rock data are used to evaluate petrogenetic hypotheses for the melt formation and to compare the unusual high-K rocks with similar igneous products from different tectonic environments.

Geochemically similar magmas, with high-K and significantly enriched in large-ion lithophile element (LILE) abundances compared to MORB, are generally tectonically linked to subduction and collision zones such as the Andes (e.g., Defant and Drummond, 1990; Kay and Mahlburg Kay, 2002) and Himalayas (e.g., Chung et al., 2003). LILE enrichment in these subduction systems is generally linked to metasomatic processes, due to the injection of fluids from the metamorphosed subducting slab. However, the occurrence of K-rich melts is also known from within plate melting anomalies. Iddings (1895) first described the shoshonitic rock series - not from a subduction setting, but within the Yellowstone province. Joplin (1965; 1968) highlighted the compositional resemblance between the shoshonitic rocks described in Iddings (1895) and the latites from the Sierra Nevada in California. Elkins-Tanton and Grove (2003) experimentally proved that such high-K melts in the Sierra Nevada are high-pressure hydrous melting products. The results of Elkins-Tanton and Grove (2003) are consistent with delamination of the lower lithosphere under the Southern Sierra Nevada (California) just prior to the eruption of these K-rich, fluid-metasomatized mantle melts in the Pliocene. It is however not known how their delamination model should be modified to incorporate the recently imaged slab-remnant beneath the Southern Sierra Nevada (Wang et al., 2013). We argue below that the geochemically similar K-rich magmas in Virginia erupted during a similar tectonic process (continental lithosphere destabilization) in an extensional setting far away from any subduction zone around the time of continental breakup between Africa and North America. Any metasomatism coincident with the melting in our study area is interpreted to be exclusively restricted to interaction of the sinking lithosphere with the surrounding asthenosphere.

The Peri-Atlantic Alkaline Pulse (PAAP)

Alkaline magmatism with ages between 250 to 50 Ma is spread over all Southern and Central Atlantic margins. Matton and Jébrak (2009) regrouped the activity between 125 and 80 Ma as the Peri-Atlantic Alkaline Pulse (PAAP). They suggested that PAAP intrusives are generally localized along pre-existing lithospheric weaknesses and/or lineaments. In contrast to LIPs, PAAP magmatism is neither spatially connected nor is the emplacement restricted to a short period in geologic time. The PAAP activity is contemporaneous to the postulated mid-Cretaceous superplume in the area (Larson, 1991). Matton and Jébrak (2009) linked these scattered alkaline activities to reactivations of crustal structures during tectonic events within the Atlantic area: (a) opening of the South Atlantic at ca. 125 Ma, and (b) a second peak of magmatism around 80 Ma during a major plate reorganization. This conceptual model for the younger events does not explain the older (to 250 Ma) alkaline activities in the circum Atlantic nor the younger (ca. 55 Ma) events.

3. Valley and Ridge Province magmatic rocks and sampling

Triassic-Jurassic excessive volcanism of the CAMP event is recorded in igneous rocks along the Atlantic rifted margins of North America, South America, Africa and

Europe (e.g., McHone, 1996; Marzoli et al., 1999; 2011; Schlische and Whitjack, 2003; Hames et al., 2003). Hames et al. (2003) reported that CAMP magmas are dominantly tholeiitic, and small regional compositional heterogeneities have been related to local differences in the lithospheric composition and/or crustal contamination. The Jurassic (Zartman et al., 1967) high-K igneous rocks analyzed in this study are however surrounded in central Appalachia by Jurassic quartz and olivine tholeiitic basalts (dolerites) to the north, east, and south (Pegram, 1990; Grossman et al., 1991; Ragland et al., 1992; Callegaro et al., 2013), and to the west by Eocene calc-alkaline basalts and andesites in Highland County, Virginia (Meyer et al., 2011; Mazza et al., 2014). The 29 samples of high-K intrusions of this study are confined to a ca. 1000 km^2 elliptical area covering most of Augusta County in western Virginia (Fig. 1). Similar to the proximate Jurassic tholeiitic dykes, the studied intrusions also have nearly an identical northwest-southeast trend (de Boer, 1967). This points toward the same far field stress during the emplacement of both magma types (Beutel et al., 2005). Alkaline igneous activity following Atlantic breakup is on the North American side not restricted to this area in Virginia but is also reported from the Monteregian Hills and White Mountain Alkaline Igneous Province (Eby, 1987) in New Hampshire.

The age of Si-rich and Si-poor K-rich rock types in Virginia is estimated to be ~150 ± 10 Ma (Zartman et al., 1967; Marvin, 1968) based on hornblende K-Ar data. This is significantly younger than the major CAMP magmatic activity, which has recently been dated with high precision zircon U-Pb data to four discrete CAMP pulses around 201 Ma and of slightly different chemistry (Blackburn et al., 2013). This age predates the above-described PAAP magmatism (Matton and Jébrak, 2009) by at least 25 My. Salters et al. (2003) reported that the CAMP dykes are difficult to date, and that ages acquired with K-Ar are providing typically younger ages in the CAMP, as this technique is highly sensitive to secondary alteration and crustal contamination. We resampled both locations where radiometric age determinations have been performed. The high-Si rock (sample: Stan2A) has been dated by Zartman et al. (1967) to 153±8 Ma, however we measured a significant loss on ignition (LOI) of > 5 wt.% for this sample. This does not support the conclusion of Zartman et al. (1967) that this dyke would be free of alteration or metamorphic overprints. We found that this sample has one of the highest LOI contents from the sample set studied here, and so seems to be one of the most altered rocks. In contrast, the resampled low-Si rock (sample: Stan8A) dated to 151±10 Ma (Marvin, 1968) shows petrographically and geochemically the least alteration from the studied rock succession. Both magma types are contemporaneous, as confirmed by mixing at a cross cutting interface of a high-Si dyke and a low-Si dyke (Johnson et al., 1971).

Paleomagnetic evidence for a relation between the dykes studied here and the typical tholeiitic CAMP dykes has been provided by de Boer (1967). He studied 7 cores from K-rich dykes and reports paleomagnetic evidence that these dykes and the other studied Appalachian dykes belong to igneous activity in the Jurassic. As the K-Ar method provides typically younger ages in the CAMP (Salters et al., 2003), we assume that the real crystallization ages of the intrusions are probably slightly older than the ages previously suggested in Zartman et al. (1967) and Marvin (1968) until new radiometric age data become available. We note that our geodynamic models (described below) predict that mantle lithosphere instabilities start to develop during continental rifting, and detachment occurs after breakup. The dykes that we study here are thus predicted to be younger than the primary CAMP age. Nevertheless, the present age constraints are not as strong as we would like to see, and more work is

needed. The intrusions studied are not well exposed, and the field guide by Johnson et al. (1971) has been used to define sample locations of interest (Fig. 1). In contrast to contemporaneous and chemically similar igneous rocks outcropping within the Monteregian Hills and White Mountain Alkaline Igneous Province (Eby, 1987) in New Hampshire, the outcrops studied here are all dykes just a few meters wide and up to a kilometer in length with porphyritic texture. We list in the petrology paragraph (4.1.2.) only major petrographic characteristics; detailed field descriptions and petrographic observations of the studied rocks can be found in Johnson et al. (1971).

4. Petrology and Geochemistry

4.1.1 Analytical geochemistry

Rock samples were prepared in the manner described by Meyer et al. (2009), and the whole-rock major element geochemical data were determined by XRF with a Phillips PW 2400 using the method described by Meyer et al. (2002). A new low blank high temperature HF-HNO_3 digestion procedure (Haaga, 2014) of 100 mg sample powder was used to determine whole-rock trace elements, including the Rare Earth Elements (REE), with the Thermo-Finnigan Element2 HR-ICP-MS at the University of Bergen Department of Earth Science. International reference rocks were prepared using the same sample preparation procedure for calibration while two CAMP standard rocks and a basalt were used as a quality control. Tables 1 and 2 list the major element abundances in wt.% and trace elements in ppm. As quality control on our new trace elements, we measured three USGS international standards (BCR-2; Columbia River Basalt, DNC-1 Durham, North Carolina dolerite, W-2 Centreville Virginia diabase) identical to our unknown samples. The accuracy (% recovery) for most trace elements is very good (Table 3).

4.1.2. Petrographic descriptions

Generally, the Si-rich igneous rocks are medium grained hypidiomorphic and equigranular with potassic feldspar phenocrysts and lesser biotite and hornblende in a groundmass of euhedral nepheline and acmite. Based on the small optical angle (2V), the potassic feldspar appears to be primarily sanidine; the high temperature and fast cooling potassic feldspar variety. In several samples, nepheline crystals have partially to completely been replaced by natrolite and/or analcite. The low-Si adakitic rocks are massive dark igneous rocks composed of euhedral, hornblende, biotite and more rarely olivine (serpentine) and titanaugite phenocrysts. The groundmass is composed of poorly crystallized plagioclase or more rarely feldspathoids, and the minor accessory phases are opaque (Fe-oxide) minerals. High-Si rocks tend to show higher alteration characteristics compared to the low-Si rocks, where alteration seems limited to serpentinisation and vugs of analcime/calcite.

4.2 Geochemical observations

The igneous rock succession studied, which is bi-modal in character (high-Si (SiO_2 >54.82 wt.%) and low-Si (SiO_2 <48.86 wt.%)), has distinguishing higher concentrations of Na_2O (8.04 – 11.45 and 1.08 – 5.19 wt.%), K_2O (5.23 – 6.61 and 2.72 – 4.99 wt.%), Al_2O_3 (19.77 – 23.9 and 12.7 – 17.79 wt.%), and P_2O_5 (up to 1.7 wt. %) than other CAMP magmas (Merle et al., 2014; Grossman et al., 1991) and/or the nearby Eocene volcanics. The studied rocks have major element characteristics much more similar to subduction related shoshonitic and adakitic melts compared to classical rift-to-drift related magmas (Fig. 2). The K_2O vs. SiO_2 diagram (Fig. 2) also shows that the high-K affinity of the melts observed in this study is probably not an exotic unique case within the CAMP. However, such dominant K_2O abundances in alkaline rocks could also be due to metamorphic substitution of potassium for sodium. To confirm the intrinsic high-K melt nature of the samples, we used the diagram of Th

vs. Co (Fig. 3) to classify altered volcanic island arc rocks (Hastie et al., 2007). The variation of these two trace elements is not fractionated during post-magmatic processes and so verifies the petrogenetic character of the sampled rock series as primitive and evolved high-K melts. Interestingly, a significant part of published CAMP rocks (http://georoc.mpch-mainz.gwdg.de/georoc; CAMP.csv) with a higher K_2O content (>1 wt. %) from within the U.S. follows the same trend as the magmas studied here. These major and trace element characteristics are consistent with geochemical characteristics of delamination magmas (Kay and Mahlburg Kay, 1993).

4.3 Interpretation of geochemistry

Kay and Mahlburg-Kay (1993) pointed out that some evolved delamination magmas share geochemical features (high La/Yb ratio and Sr content) with experimentally synthetized melts from a subducting slab (Defant and Drummond, 1990). This has been explained by the fact that in both delamination and subduction, melting of an eclogitic garnet-bearing mafic rock occurs at high pressures. Xu et al. (2002) first described adakitic rocks from a non-arc environment by substituting the slab melting process from the classical adakitic magmatism concept with down-dripping lower-crustal fusion. Prior to their study lower crustal melting had already been proposed for some adakitic rocks in arc settings (Atherton and Petford, 1993) but could not be separated from slab melting.

Smithies (2000) emphasized that most TTGs have lower Mg numbers than adakites. In addition, other compatible element concentrations (e.g. Ni and Cr) could discriminate between lower crustal melting and slab melting. Condie (2005) deducted that most TTGs, although partial melts of hydrous mafic sources, have not interacted with the mantle wedge. He further showed that there is more overlap in terms of Cr and Ni distributions but a large number of TTGs has lower Ni and Cr content than adakites. Unfortunately such an interpretation is not unique and works only for an in-situ lower crustal melting end-member event. In a geodynamic system with a hydrated lithospheric instability, lower crustal melts from the sinking body might actually interact with ambient mantle.

We favor a delamination model for the Virginia adakites because of the extensive rifting prior to breakup, which facilitated formation of lithospheric instabilities; there are no indications from other rifted margins that adakites would form during the emplacement of magmatic bodies ("High Velocity Lower Crustal Bodies") during margin formation, as described in Atherton and Petford (1993).

Meyer et al. (2009) showed that at the Norwegian Vøring margin and along the NE Atlantic margins in general, crustal anatexis, prior to the emplacement of the Seaward Dipping Reflector Sequence, is a systematic magmatic stage in the development of a magmatic rifted margin. However, this mantle-crust interaction is spatially much closer to the developing oceanic crust than the adakitic magmatic activity on the Virginia margin, and the melting lithologies are generally upper to middle crustal rocks at the Norwegian margin. High velocity lower crustal bodies (HVLC) at the mantle crust transition are characteristically detected seismically in magmatic rifted margins (Eldholm et al., 2000). If adakite formation is to be linked to the emplacement of these asthenospheric melts at the base of the crust, partial lower crustal fusion and adakitic melts should accompany HVLC bodies along the margin. However, the present study is to our knowledge the first report of adakitic rocks from a continental breakup setting, which suggests that this lower crustal melting process is probably of minor importance.

An alternative explanation for adakitic rock petrogenesis was proposed by Castillo et al. (1999) with a petrologic assimilation-fractional crystallization (AFC)

model. The AFC following magmatic evolution studied by Castillo et al. (1999) shows the expected increase in LREE between the primary basaltic and the evolved magmas; the opposite has been observed in our studied rock succession (Fig. 6). By analogy to the rocks described in Xu et al. (2002), the Virginia magmatic system is clearly bimodal in major and trace element geochemistry with, for example, an SiO_2 gap from 50 to 56 wt.%. This feature seems not to be linked to a sampling bias because in a relatively small magmatic system such as that described here, one would assume the full melt evolution is sampled and not just two end-members. An example is sample Stan20A which is a high-Si melt with the highest observed Th content (Fig. 2) and a distinct negative Eu-anomaly in its REE pattern due to plagioclase fractional crystallization.

There is one major difference between our samples, "classical" volcanic arc adakites, and the pure experimental melts of a metagrabbro. The term adakite was originally proposed by Defant and Drumond (1990) to define silica-rich ($\geq$ 56 wt.% SiO_2), high Sr/Y and high La/Yb volcanic and plutonic rocks derived from melting the subducting slab (Castillo, 2006). These geochemical characteristics are consistent with the Virginia "evolved" high-silica samples (Fig. 2) but not with the low silica rocks ($\leq$ 50 wt.% SiO_2). Such low-Si rocks with trace element abundance patterns similar to those of "classical" adakites, but with higher enrichments in incompatible elements and a significantly higher Mg#, are also known from arc environments (e.g. Castillo, 2006; 2012), where they are believed to be petrogenetically associated to adakitic melts interacting with the mantle. Experiments have shown that such high Mg# melts are not in equilibrium with a melt from a basaltic source; these melts need to have interacted with material more mafic than basalt (Smithies, 2000). In addition to the anomalous Mg contents for adakites, Kay (1978) used the high Ni abundances of igneous rocks from Adak to retrace mantle interaction for these melts. Rapp et al. (1999) experimentally studied the interaction of primary Si-rich eclogized ocean crust melts with peridotite and concluded that the modally and/or cryptically metasomatized mantle is the likeliest source for these low silica and high Mg# melts. In a global study of adakites Martin et al. (2005) confirmed the two distinct compositional high- and low-silica adakite groups and their plausible melting sources defined by Rapp et al. (1999). Fig. 1 illustrates that both melt types were generated within the area encompassed by the CAMP at the rift-to-drift transition of the Atlantic margin. In comparison to the typical high Si adakites, the low silica rocks have (1) higher LREE to the HREE enrichments; (2) show significantly higher Sr contents (2473 – 1057 ppm vs. 661 – 71 ppm); (3) are relatively poor in Rb (35 – 97 ppm vs. 153 – 267 ppm) (cf. Table 2; Fig. 2, 3, 6).

The compositional gap between 50 to 56 wt. % SiO_2 is best explained by "contamination" of adakite with mantle peridotite by assimilation (of peridotite) and fractional crystallization (of orthopyroxene and garnet) (Yogodzinski et al., 1995; Rapp et al., 1999). For example, Rapp et al. (1999) showed experimentally that assimilating 16% peridotite is enough for a Si-rich adakitic melt to lower the SiO_2 content substantially (>5 wt.%). In the diagram CaO vs. SiO_2 (Fig. 7) we not only replicate the close petrogenetic relation between our high-Si adakites with synthetic partial melts of a meta-basalt (Fig. 4); our low-Si samples follow the same trend as recent experiments by Mallik and Dasgupta (2013; 2014) studying the interaction of eclogite derived melts with lherzolite at 3 GPa and different CO_2 contents. Mallik and Dasgupta (2013; 2014) observed that a felsic andesite changes through interaction with the garnet bearing lherzolite to mafic basanite and nephelinite.

Some of our melts are clearly enriched in CO_2. Dasgupta et al. (2007) synthetized a compositionally similar primary melt. However they needed a 5 wt.% carbonate bearing fertile peridotite to do so. Also during the andesite lherzolite reactions a significant increase in CO_2 is necessary for producing such CaO rich (> 10 wt. %) and low SiO_2 (<45 wt. %) melts (Mallik and Dasgupta, 2013). However, such high carbonate contents are unlikely in a fresh lherzolitic mantle and clearly point to interactions of the mantle with carbonate rich rocks, fluids or melts prior or during to the melting of these CO_2-enriched melts. Recycling of crustal material back into the mantle is the most plausible process for carbonate enrichment.

One of our samples has geochemical similarities to experimental garnet-lherzolite primary melts (Walter, 1998; Herzberg, 2006). We modeled using Petrolog software (http://petrolog.web.ru; Danyushevsky and Plechov, 2011) a liquid line of descent (LLD) which suggests that such differentiation would result in a completely different magmatic series as observed in Virginia. In contrast, the variation points clearly towards a dehydration melting of a basaltic lithology followed by interaction of these partial melts with garnet-lherzolite and CO_2.

The Virginia low-Si rocks can be linked to low silica adakites, while the siliceous samples are characterized as pure adakitic partial melts of a lower crustal rock (Fig. 4, 7). Calculated melting curves of metamorphosed and hydrated oceanic crustal material, with MORB composition can reproduce the observed geochemical variations within the Virginia high-Si igneous rocks (Fig. 4).

Following the work of Pegram (1990) and Puffer (2003) who studied the source of CAMP magmas, we used for further modeling of our trace elements a continental arc composition from Rudnick and Gao (2003) to represent our geochemical source composition. Trace element patterns (Fig. 5) were calculated with a non-modal fractional melting model (Shaw, 2006). The partition coefficients have been calculated from the "Geochemical Earth Reference Model – GERM" database (http://earthref.org). This model further comprises a hydrated meta-basaltic composition consisting of amphibole + clinopyroxene + garnet + magnetite + apatite. In addition to garnet, this mineralogy is consistent with metagabbros outcropping in Lynchburg, Virginia (Conley, 1985). The eclogitic source material must have had a high amphibole modal content with amphibole and garnet as residual phases in the source. The best fit with LILE (Cs to K), HFSE (Zr), and REE (Ce to Lu) abundances of the Si-rich adakites and our non-modal batch melting model calculations is provided with a 10% degree of melting of lower crustal material (Fig. 5). Smaller differences within the group of high-Si rocks are due to variable partial melting degrees.

The low-Si rocks studied are significantly different from similar low Si, Rb and high Sr containing Algarve Basin (Portugal) CAMP dykes (Martins et al., 2008). The geochemical characteristics of these Algarve high Sr-dykes have been linked by Callegaro et al. (2014) to shallow assimilation of carbonate by a typical CAMP tholeiitic melt. However, in contrast to the rocks studied here, the REE geochemistry of the Portuguese melts follows the slight (ca. 1.5x) $LREE_N/HREE_N$ enrichment of CAMP tholeiites and not the excessive (ca. 80x) adakite $LREE_N/HREE_N$ enrichment with similar $HREE_N$ contents (Fig. 6). This difference with much lower K content in the Portuguese igneous rocks discards a similar source and points toward systematically different petrogenetic histories for both CAMP magma types. While the REE geochemistry of the Algave melts points towards a shallow source, the rocks studied here descend from processes within the garnet stability field.

The observed parallel REE pattern variation within the low-Si rocks (Fig. 6) illustrates the evolution described by Malik and Dasgupta (2014) from andesite to nephelinite while interacting at different depths with lherzolite starting with garnet lherzolite (garnet and orthopyroxene crystallization) followed at shallower depth by orthopyroxene crystallization. The close major element geochemistry between the measured low-Si adakites and the reaction product melts reported from Mallik and Dasgupta (2014) suggests that this process is plausible.

As some magmas had to be enriched in CO_2 (Fig. 7) volatiles played a major role in the petrogenesis of these magmas. However, the effect of volatile components on the batch melting models used has not been considered explicitly in order to keep the petrogenetic models simple. It is well known that the presence of H_2O and/or CO_2 lowers the liquidus and solidus temperature drastically. In our delamination model, shallow asthenospheric melting is induced not only by decompression but also as a result of the fluid injection into the asthenosphere by the sinking of a dehydrating amphibolitic lithology (drip). As a result, some of the low-Si rocks are mixtures between adakitic melts and dehydration melting of asthenosphere. Our calculations with a simple theoretical non-modal batch melting model show that melting degrees of 5 to 10% of a (metasomatically overprinted with dehydration fluids and/or melts) spinel-lherzolite (55% olivine, 25% orthopyroxene, 11% clinopyroxene and 9% spinel) is also able to reproduce the observed REE patterns in the low-Si adakites (Fig. 6). Interestingly, the observed steep REE patterns in this model are not due to melting within the garnet lherzolite field, as the variation in C1 normalized HREE is too large to have garnet as a residual phase. This steep REE pattern is a "fingerprint" of the initially delaminating and dehydrating garnet bearing eclogite and its metasomatisation with high-Si adakites and fluids of the asthenosphere. The reactivated back-arc source signature within the majority of CAMP reported by Puffer (2003) could be due to a similar metasomatic overprint of the asthenosphere during delamination induced lithospheric thinning. We note that samples studied by Merle et al. (2013) from the lower CAMP unit of the Orange Mt. Group (e.g. the lower Palisades sill) also have a much steeper REE pattern than the typical CAMP tholeiites (Fig. 6). This suggests that the geochemical diversity of CAMP magmas seems to be more important than previously thought.

We propose that the above described geochemical similarities between the rift-to-drift transition rocks we studied, and high-/low-silica adakites, as well as experimental constraints on high pressure slab melting (e.g. Rapp et al., 1999) provide a strong case that these Virginia intrusions have been produced either directly (high silica) or indirectly (low-silica) by fusion of mafic down-dripping lithospheric material. Petrologically the delaminated material during the rift-to-drift transition below Virginia could be a trapped Ordovician (Taconic) amphibole-dominated eclogite that was not fully dehydrated and did not undergo partial melting.

5. A model for breakup-related delamination and adakite formation on the U.S. East Coast

Sleep (2007) proposed that continental mantle lithosphere may become unstable during rifting as a result of large lateral thermal gradients that develop between the rift and adjacent un-deformed lithosphere. Section 5.2 describes simple models of this process and shows that an instability matures to become a delamination by foundering of lower crust and mantle material. In the Valley and Ridge province, ophiolites were emplaced in the crust (section 5.1). Adakites formed upon melting of the ophiolite-interspersed crust following delamination.

539 **5.1 Constraints on ophiolitic slabs trapped below Virginia during collisional**
540 **orogens**
541 Mantle xenoliths from kimberlites provide the best petrological map of the
542 subcontinental lithosphere composition. Mount Horeb (Fig. 1) is a post-Middle
543 Ordovician kimberlite in the study area that sampled the lithosphere prior to the
544 emplacement of the K-rich dykes (Meyer, 1976). Based on lherzolitic garnets Griffin
545 et al. (2004) define the SCLM beneath Mt. Horeb as fertile mantle with a limited
546 thickness of around 110 km. They further postulate that the SCLM in the area was
547 formed during the Grenville orogeny. Presently accepted tectonic models of the
548 Valley and Ridge province (Fig. 1) suggest that at least part of the post-Greenville
549 sequence consists of mafic to ultramafic packages emplaced on Laurentia (Wang and
550 Glover, 1997). To explain the linear occurrence of eclogite, retrograde eclogite,
551 peridotite and migmatitic basement gneisses in the nearby southern Blue Ridge,
552 geodynamic interpretations require the closure of a small oceanic basin in the area
553 (e.g. Anderson and Moecher, 2009; Sinha et al., 2012). This linear array of meta-
554 ultramafic rocks in the Blue Ridge Belt is recognized as an Ordovician (Taconic)
555 suture (e.g. Raymond et al., 2003). The chain of ultramafic bodies lies southeast of the
556 ≥1 Ga basement massifs and can be followed from Alabama in the south to
557 Newfoundland in the north (Hibbard et al., 2006). The Lynchburg Group, with its
558 type locality at Lynchburg (around 150 km SE from our study area), also includes
559 ultramafic-metagabbro-metabasalt sequences, which have been interpreted as
560 dissembled ophiolitic sequence (Conley, 1985; 1986). The metagabbros described by
561 Conley (1985) from the Lynchburg formation "*…are composed of actinolite (in part*
562 *uralitic amphibole), albite, epidote chlorite and minor amounts of zircon, quartz,*
563 *sphene, ilmenite and magnetite…*".
564 Wang and Glover (1997) report some garnet bearing lithologies from the
565 Lynchburg Group and they define an amphibole content of 50 to 65% within the
566 meta-volcanic to subvolcanic rocks. They question the ophiolitic nature of this mafic
567 to ultramafic rock succession in the Lynchburg Group and prefer to associate them
568 with a Late Iapetan rifting event. However, Wang and Glover (1997) already
569 concluded that the observed abundance of supracrustal ultramafic rock emplaced
570 during a rift stage is "*perhaps an anomalous, but interesting, addition to the tectonic*
571 *lithofacies assemblages in rift basins*". We favor here a very slow spreading ridge
572 nature for the Valley and Ridge ophiolites as suggested by Raymond et al. (2003).
573 Raymond et al. (2003) also suggested that these ancient slow spreading oceanic
574 lithospheres were deformed, fragmented and metamorphosed during the Taconic
575 orogenesis and hydrated during Late Taconic, Acadian and Alleghenian
576 metamorphism. It is likely that such oceanic lithosphere was not only trapped within
577 the present upper crustal segment but was also emplaced in the lower crust and the
578 lithospheric mantle. Such a lithosphere fulfills the prerequisites to form hydrous
579 eclogitic gravitational instabilities in an extensional setting.
580 To test the plausibility of our petrogenetic model for the high-K magmas in
581 Virginia, we used geodynamic models of lithosphere-asthenosphere interactions
582 during rifting. These models not only cast light on the lithospheric instabilities, but
583 show possible physical conditions during lithospheric recycling in the upper mantle.
584 **5.2 Geodynamic models of margin instabilities**
585 The traditional rift model (McKenzie, 1978) assumes that the mantle
586 lithosphere thins approximately in similar proportions to the crust. However, as Sleep
587 (2007) illustrated, larger lithospheric portions may be recycled back into the
588 convecting mantle by gravitational instabilities that form towards the end of the syn-

589 rift stage. This would result in rift/margin uplift, as mantle lithosphere material is
590 replaced by less dense asthenosphere, and melting that continues after continent
591 fragmentation (Esedo et al., 2012).
592 We first describe an upper-mantle scale numerical model used to study the
593 formation of lithospheric drips during the late stages of continental rifting. Small-
594 scale convection cells develop below the rift zone that bring lithospheric mantle
595 material down below the rift margins. By formation of these lithospheric
596 downwellings lithosphere is removed from below the margins and the lithosphere is
597 thus thinned more than it would have been by lithosphere extension alone. A second
598 set of models was used to understand lithospheric deformation during foundering in
599 more detail. These models show how an instability develops into a delamination,
600 removing lower crustal and mantle lithosphere material.
601 *Upper-mantle scale model of rift instabilities*
602 The finite-element software CitCom (Moresi and Gurnis 1996; Zhong et al.,
603 2000, van Hunen et al., 2005) was used to model rifting and formation of instabilities
604 beneath rift margins. In these models, mantle flow and lithosphere deformation are
605 described by solving the equations of conservation of mass, momentum and thermal
606 energy with the Boussinesq approximation. A visco-plastic rheology is included (van
607 Wijk et al., 2010; van Hunen and Allen, 2011) that combines a pseudo-plastic
608 rheology for Byerlee's law with viscous deformation. Adiabatic heating/cooling is
609 included in the models. The model domain is two-dimensional, 660 km deep and
610 about 1500 km wide, with a typical 5-7 km resolution, and consists of a (thermally-
611 defined) high-viscosity lithosphere (up to $1 \cdot 10^{24}$ Pa s) overlying a low-viscosity
612 asthenosphere and upper mantle. A small weakness was introduced in the center of
613 the model domain as a seed for localizing rifting. Boundary conditions include
614 imposed velocity boundary conditions on both sides of the domain to extend the
615 lithosphere. These taper to zero in the asthenosphere (Fig. 8). Thermal boundary
616 conditions are zero heat flux at the side boundaries, and constant temperature at the
617 top and bottom (0°C and 1350°C). A diffusion or dislocation creep viscous rheology
618 is used with activation energy and volume of E*=360 kJ/mol and V*=5 cm^3/mol. The
619 reference viscosity at reference depth z_r=660 km and reference mantle temperature
620 Tm=1350°C was $1.76 \cdot 10^{21}$ Pa s at the base of the model. This results in a sub-
621 lithospheric mantle with a minimum viscosity of ~$5 \cdot 10^{19}$ Pa s.
622 We performed a series of tests in which the mantle rheology was varied
623 between power law exponent=1 and stress dependent, and the extension rate,
624 thickness of the lithosphere and activation energy were varied between 8 and 24
625 mm/yr, 120 and 140 km, 180 and 360 kJ/mole, respectively. Shown and discussed
626 hereafter are results with extension velocity 16 mm/yr, stress dependent rheology with
627 power law exponent n=3.5, 140 km thick lithosphere, activation energy E*=360 and
628 kJ/mole, activation volume V*=5 cm^3/mole. None of these parameters varied changed
629 in a major way the pattern of instability formation or mantle flow pattern, except for
630 a) the activation energy, which affects the formation of instabilities, as discussed
631 hereafter, and b) absolute mantle viscosity, since increasing mantle viscosity by a
632 factor 10 impedes the formation of gravitational instabilities (van Hunen et al., 2005).
633 Negative buoyancy is a function of temperature only; the thermal expansion
634 coefficient was $3.5 \cdot 10^{-5}$ K^{-1}, specific heat was 1250 J/kg/K and thermal diffusivity
635 was $1.0 \cdot 10^{-6}$ $m^2 s^{-1}$.
636 The models show that lithosphere thins upon extension and a rift is formed in
637 the center of the domain. Asthenosphere wells up below the rift and replaces the
638 mantle lithosphere (Fig. 8). The depth from which the asthenosphere wells up varies

639 during development of the rift; from quite shallow depths (~250 km or less) in the
640 early rifting stage to transition zone depths (~400 km) when the rift is well developed,
641 and deeper when the instabilities sink into the transition zone. The lateral extent of the
642 region in the asthenosphere that is involved in the rifting is ~600 km wide around
643 breakup time, including the instabilities, i.e. the rift's outermost margins. This width
644 is several hundred kilometers larger than the typical crustal width of a narrow
645 continental rift zone. When the steep topography of the lithospheric base is formed
646 during extension, gravitational instabilities form easily below the margins of the rift,
647 and small-scale convection cells develop within the rift zone as a result of the large
648 lateral thermal gradients (Fig. 8B) combined with low viscosity. They bring
649 asthenosphere up below the rift to replaces the mantle lithosphere, while below the
650 margins lithospheric gravitational instabilities ('drips') form.
651 During advanced stages of continental rifting, the convection cells that are
652 induced by the rifting lithosphere increase in size and extend into the transition zone.
653 At this time, there is mass transport between the transition zone and the
654 asthenosphere. The upwelling part of the cell transports material from the transition
655 zone into the asthenosphere and eventually possibly into the decompression-melting
656 window of the rift zone (McKenzie and Bickle, 1988). This provides a mechanism
657 whereby low-degree partial melts of transition-zone mantle may form. Additionally,
658 melting of the downwelling drips on the sides of the rift may produce some of the
659 characteristic deep-seated primary alkalic magmas found in rifts: carbonatites, and
660 nephelinites, which provide evidence for interaction of continental material with high
661 temperatures (Fig. 8) (e.g. Furman et al. 2006; Schmincke, 2007). Interestingly, such
662 volcanism is commonly found on the edges of the rift systems such as the
663 Rheingraben and the E-African rift, but not in the centers of rifts.
664 The growing instabilities below the margins of the rift migrate land-ward as
665 they develop over several hundred kilometers. They sink into the asthenosphere as a
666 drips and eventually detach. The mantle lithosphere is thinned overall below the
667 margins of the rift because its material was consumed to form the drips. When the
668 detaching lithosphere material sinks into the transition zone, a counterflow develops
669 (Fig. 8C) that brings significant amounts of transition zone material up. This warm
670 material, brought to shallow depths below the rifted margins, may supply magmatic
671 activity on rifted margins for millions of years after continental rupture, as observed
672 for example on the Newfoundland passive continental margin (Peron-Pinvidic et al.,
673 2010). We did not calculate volumes of magma, but expect modest amounts.
674 Detachment of the drips occurs several hundred kilometers inland from the continent-
675 ocean boundary.
676 Instabilities formed in all models where the set of rheological parameters
677 discussed above was used. Extension rate and initial weak seed width (which affects
678 the width of the rift zone to be formed) did not affect the formation or development of
679 the downwellings. Instabilities did not develop when the viscosity was increased by
680 an order of magnitude. In this case the rift zone still formed, but without the formation
681 of instabilities. Downwellings developed more easily when the activation energy was
682 lowered to 180 kJ/mole, because the thickness of the rheological boundary layer
683 beneath the lithosphere affects the vigor of small-scale convection and formation of
684 downwellings or drips (Huang et al., 2003, van Hunen et al., 2005). Lowering the
685 activation energy reduces the dependence of viscosity on temperature such that a
686 thicker boundary layer is formed at the base of the lithosphere.
687 When instabilities develop, the mantle lithosphere of the margins is thinned
688 more (Fig. 8C) than the upper crust. This has previously been described as "depth-

dependent thinning" (Driscoll and Karner, 1998; Davis and Kusznir, 2004). Depth-dependent thinning (DDT) has been explained conceptually by different processes. The amount of mantle lithosphere thinning during rifting is determined from the calculated thermal subsidence that a rift has undergone and if the thermal subsidence exceeds normal expected values (crustal values) DDT is inferred. Buck (2004) therefore explained DDT by replacement below the margins of low density asthenosphere with normal mantle. While still present, the low density asthenosphere would hold the lithosphere up, and when replaced by normal mantle, 'extra' subsidence would follow. Driscoll and Karner (1998) proposed the development of a shear zone in the crust that could offset upper crustal thinning from lower crustal and mantle lithosphere thinning over long distances. Highly thinned mantle lithosphere would then underlie barely thinned upper crust. Kusznir and Karner (2007) explain DDT by a model in which mantle lithosphere is removed by a divergent upwelling mantle flow. In their model, rifting and breakup result from an upwelling divergent flow field that actively drives lithosphere deformation and separation. The divergent flow field would thin the mantle lithosphere more than the crust, with DDT as a result. Here we find that DDT can be explained by loss of lithosphere during the later stages of rifting.

To summarize, mantle lithosphere instabilities may form below rift margins when conditions of the upper mantle (viscosity, rheology) are favorable. The high-density eclogites of the Valley and Ridge province probably assisted in de-stabilizing the margin mantle lithosphere.

Model of onset of delamination below the East Coast margin

The lithosphere instabilities below the U.S. East Coast margin start in our models (Fig. 8, 9) as gravitational instabilities or drips, but eventually they result in delamination of lower crustal and mantle lithosphere material (Fig. 9B). We used a model of lithosphere deformation with a rheologically layered lithosphere to illustrate this process.

A particle-in-cell finite element code (Gale; Moresi et al., 2003) was used to study lithosphere deformation below the margin of a rift. The model setup (Fig. 9A) consists of thinned lithosphere (as a result of rifting) adjacent to normal thickness lithosphere. Below the margin of the rift an instability grows, that will eventually delaminate from the continental margin. The brittle upper crust deforms following a Drucker-Prager failure criterion. Brittle parameters, representing values for continental crust (taken from Byerlee, 1978; Jaeger and Cook, 1979; Turcotte and Schubert, 2002) included cohesion (16 MPa), cohesion after softening (3.2 MPa), internal friction angle (15º) and strain at which softening occurs (0.5). Viscosity and density are not temperature dependent. The viscosity of the brittle crust was 10^{22} Pa s, and its density 2700 kg/m^3. The lower crust was modeled as a low-viscosity layer, with a viscosity of 10^{18} Pa s and a density of 2800 kg/m^3. The mantle lithosphere had a density of 3300 kg/m^3 and a viscosity of 10^{21} Pa s. The viscous sub-lithospheric mantle had a density of 3200 kg/m^3 and a viscosity of $5*10^{20}$ Pa s. The model domain was 800 km (width) by 500 km (depth), divided into 12,000 elements. The initial brittle crust was 20 km thick, and the underlying viscous crust was 15 km thick. The mantle lithosphere was thinner in the rift (65 km) than in the undeformed lithosphere (90 km). Boundary conditions included a freely deformable surface, a free-slip bottom, and on the right and left sides of the model domain v_x and v_y (the horizontal and vertical components of the velocity field) were 0 m/s. Rheology was linear and not temperature dependent in this simplified model.

738 The model predicts that the instability is mainly fed from lithosphere below
739 the rift, in agreement with the previous models discussed above. The lower crust
740 thickens in the drip by lower crustal flow. This is possible in the models because the
741 lower crust had a low viscosity. Other tests that we performed with higher lower crust
742 viscosities (>10^{19} Pa s) did not develop a drip, but merely "sagged" the lithosphere.
743 Such low viscosities (~10^{18} Pa s) of the lower crust have been reported in for example
744 Tibet (Clark and Royden, 2000) and the western U.S. (Kruse et al., 1991), and may
745 occur where the lower crust is heated, for example as a result of rifting. The model
746 also predicted where yielding occurs, and yielding was observed at the upper crust-
747 lower crust boundary above the drip (Fig. 9B). We interpreted this as the onset of
748 delamination which is usually modeled by including a hook-shaped weak zone in the
749 lithosphere (Göğüş and Pysklywec, 2008). The zone that yields corresponded to a
750 zone of very high strain rates (indicated in Fig. 9C) and the drip seemed to detach at
751 this location. Model predicted horizontal deviatoric stresses (Fig. 9C) show that the
752 crust above the drip (the margin of the rift) was locally under compression, while the
753 rifted area extended further.
754 This simple model predicts that an instability below the margin may detach from
755 lower crustal depths, and lower crustal and mantle lithosphere material will be
756 removed from below the margin. This has implications for our model for adakite
757 formation below Virginia.
758 **5.3 Model for the formation of adakites on rifted margins**
759 Magmatism at rifted margins is dominated by asthenospheric melts generated
760 during decompression melting of upwelling asthenosphere. Magma compositions are
761 however quite diverse, giving clues about other processes that accompany rifting and
762 continent rupture. During the closure of the proto-Atlantic and its related back-arc
763 basins, the Appalachian lithosphere sampled an ophiolitic mélange within major
764 sutures. Subsequent metamorphic events in the Valley and Ridge province increased
765 the rock density of the ophiolites (eclogite) and partly hydrated these mafic-to-
766 ultramafic rocks. As our geodynamic models illustrate, such a preconditioned
767 lithosphere will likely aid in developing gravitational instabilities at the
768 asthenosphere-lithosphere boundary. After foundering, the delaminated lithosphere
769 undergoes metamorphism, heats up, and interacts with fluids and melts in the
770 surrounding convecting mantle. Partial melting of this metamorphic lithology
771 produces high-Si adakitic melts. These melts percolate upwards through the mantle
772 and were partially injected into crustal fractures. Where melt-to-peridotite
773 (asthenosphere) ratios were small, the melts and fluids leaving the sinking lithospheric
774 block became fixed within the peridotites. 5 to 10% degrees of melting of such a
775 metasomatically overprinted and fertile asthenosphere produced the low-Si adakitic
776 rocks of the Virginia adakites.
777 **6. Discussion and conclusion**
778 As Xu et al. (2002) mentioned, there are currently no geochemical criteria that
779 discriminate mafic lower crust adakitic melts from subducting slab adakitic melts, and
780 as a result, based on our geochemical analyses alone, it is not possible to determine
781 whether the delaminated material beneath Virginia was lower continental crust and/or
782 a formerly trapped slab in the lithosphere. Both scenarios provide equally plausible
783 sources for the generation of adakitic melts at a continental margin. The low-Si
784 adakitic rocks in Virginia however are not primary slab melts but had to be formed
785 from a lithosphere that was metasomatically overprinted by similar melts as the
786 studied high-Si adakites.

Recycling of lower crustal material back into the mantle has several implications. The involvement of crustal material will not only influence the melt chemistry of some rifted-margin magmas to more adakitic compositions, but this process recycles fertile material back into the mantle. Recycling of oceanic lithosphere at subduction zones includes mainly the oceanic crust/mantle and minimal upper continental crustal sediments in contrast to the process observed below the U.S. East Coast. To our knowledge, this adakite province in Virginia is the first direct evidence of rift-related adakites. However, earlier studies inferred the existence of such magmatic rocks through similar recycling scenarios. Willbold and Stracke (2010) highlight the enriched isotopic mantle signatures interpreted to result from recycling. Lustrino (2005) presented a theoretical model on how such recycled lower continental crust would influence the mantle composition and evolution. Korenaga (2004) suggested that excessive magma volumes at the rift-to-drift transition in the Atlantic can plausibly relate to upper mantle heterogeneities associated with a formerly subducted slab stored at the upper-lower mantle transition. Foulger and Anderson (2005) suggested that this model may explain the ongoing excessive melting at Iceland if the subducted slab trapped during the Caledonian continental collision delaminated during the reopening of the Atlantic.

The actual "delamination" process has until now to the best of our knowledge not been documented at a magmatic rifted margin. The adakitic melts discussed here indicate strong reactions between sinking lithospheric material and the surrounding asthenosphere, either by direct partial melting of lower crustal rocks (high silica melts), or by melt production in a fluid and melt-metasomatically overprinted asthenosphere. These interactions between sinking lithosphere and the upper mantle, in addition to further geochemical exchanges during the voyage of the lithospheric drips generate significant mineralogical and geochemical heterogeneities within the traversed mantle. Such fertile drifting lithospheric packages within the asthenosphere could be responsible for mid-plate volcanism (Anderson, 2007). We speculate that further recycling within the convecting mantle of floating fertile meta-igneous rocks that delaminated from the rifted margin could be responsible for Atlantic melting anomalies such as the Azores or Bermuda. The geological structure of the east coast of the U.S. provides enough sutures and tectonic events to trap slab material within the lithosphere and hydrate these bodies during subsequent metamorphosis. For example, Griffin et al. (2004) mapped the subcontinental lithospheric mantle beneath Virginia while studying mantle xenoliths from Mt. Horeb (located 70 km southwest of the studied igneous high-K rocks; Fig. 1). The SCLM was produced during the Grenville orogeny (Griffin et al., 2004) and provided typical Phanerozoic fertile lithosphere, significantly less depleted than other eastern North America locations (e.g. Kentucky and Pennsylvania), during the emplacement of the dykes we studied.

Analyses of adakites from a small volcanic province in Virginia suggest that gravitational instabilities may develop below rifted margins. As most volcanic rifted margins are either only accessible by scientific offshore drilling and/or in remote areas covered by blanketing lava flows, this process might have been overlooked previously. The process is important for understanding the magmatic makeup of rifted margins and the recycling history of continental lithosphere into the convective mantle by reintroducing fertile packages.

Acknowledgements

We would like to thank Don Anderson for many fruitful discussions. We further acknowledge Claire Currie, Bob Wintsch, Robert W. Kay, Sara Callegaro and Andrea

Marzoli for advice and suggestions on this manuscript, Gillian Foulger, Michele Lustrino and Scott King are thanked for their editorial work. Paul Low is thanked for help with the Virginia physiographic region map. RM thanks CGB, Rolf B. Pedersen and the W&L Geology department for support. JVW was supported by NSF-EAR 1015250. Some of the model calculations were done with Gale, a code developed by Computational Infrastructure for Geodynamics (www.geodynamics.org), Victoria Partnership for Advanced Computing (www.vpac.org), and Monash University (www.monash.edu).

References

Anderson, D.L., 2005, Large Igneous Provinces, delamination, and fertile mantle: Elements, v. 1, p. 271-275.

Anderson, D.L., 2007, The eclogite engine: Chemical geodynamics as a Galileo thermometer: The Geological Society of America, Special Paper, v. 430, p. 47-64.

Anderson, E.D., Moecher, D.P., 2009, Formation of high-pressure metabasites in the southern Appalachian Blue Ridge via continental subduction beneath the Laurentian margin: Tectonics, v. 28, TC4012, DOI: 10.1029/2008TC002319.

Atherton, M.P. and Petford, N., 1993, Generation of sodium-rich magmas from newly underplated basaltic crust: Nature, v. 362, p. 144-146.

Beutel, E.K., Nomade, S., Fronabarger, A.K., Renne, P.R., 2005, Pangea's complex breakup: A new rapidly changing stress field model: Earth and Planetary Science Letters, v. 236, 471-485.

Bird, P., 1979, Continental delamination and the Colorado Plateau: Journal of Geophysical Research, v. 84, p. 7561–7571.

Blackburn, T. J., Olsen, P. E., Bowing, S. A., McLean, N. M., Kent, D. V., Puffer, J., McHone, G., Rasbury, E. T., Et-Touhami, M., 2013, Zircon U-Pb Geochronology Links the End-Triassic Extension with the Central Atlantic Magmatic Province: Science, v. 340, p. 941-945.

Buck, W.R., 2004, Consequences of asthenospheric variability on continental rifting, *in* Rheology and deformation of the lithosphere at continental margins. Karner, G.D., Taylor, B., Driscoll, N.W., Kohlstedt, D.L. (eds) Columbia University Press, p. 1-31.

Byerlee, J., 1978, Friction of rocks: Pure and applied Geophysics, v. 116, p. 615– 626.

Callegaro, S., Marzoli, A., Bertrand, H., Chiaradia, M., Reisberg, L., Meyzen, C., Bellieni, G., Weems, R.E., Merle, R., 2013, Upper and lower crust recycling in the source of CAMP basaltic dykes from southeastern North America: Earth and Planetary Science Letters, v. 376, p. 186-199.

Callegaro, S., Rapaille, C., Marzoli, A., Bertrand, H., Chiaradia, M., Reisberg, L., Bellieni, G., Martins, L., Madeira, J., Mata, J., Youbi, N., De Min, A., Azevedo, M.R., Bensalah, M.K., 2014, Enriched mantle source for the Central Atlantic magmatic province: new supporting evidence from southwestern Europe: Lithos, v. 188, p. 15-32.

Castillo, P.R., 2006, An overview of adakite petrogenesis: Chinese Science Bulletin, v. 51, p. 258-268.

Castillo, P.R., 2012, Adakite petrogenesis: Lithos, v. 134-135, p. 304-316, DOI: 10.1016/j.lithos.2011.09.013.

Castillo, P.R., Janney, P.E., Solidum, R.U., 1999, Petrology and geochemistry of Camiguin Island, southern Philippines: insights to the source of adakites and

other lavas in a complex arc setting: Contributions to Mineralogy and Petrology, v. 134, p. 33-51.
Chung, S.L., Liu, D., Ji, J., Chu, M.F., Lee, H.Y., Wen, D.J., Lo, C.H., Lee, T.Y., Qian, Q., and Zhang, Q., 2003, Adakites from continental collision zones: Melting of thickened lower crust beneath southern Tibet: Geology, v. 31, p. 1021-1024, doi: 10.1130/G19796.1.
Clark, M., and Royden, L., 2000, Topographic ooze: building the eastern margin of Tibet by lower crustal flow: Geology, v. 28, p. 703-706.
Condie, K., 2005, TTGs and adakites: are they both slab melts?: Lithos, v. 80, p. 33-44, doi: doi:10.1016/j.lithos.2003.11.001.
Conley, J.F., 1986, Ophiolites (?) in the Lynchburg Group near Rocky Mount, Virginia. In: Neathery, T.L. (ed.) Centennial Field Guide - Southeastern Section of The Geological Society of America, v. 6, p. 215-216.
Conley, J.F., 1985, Geology of the Southwestern Virginia Piedmont: Virginia Division of Mineral Resources Publication 59, p. 33.
Conrad, C.P., and Molnar, P., 1997, The growth of Rayleigh-Taylor-type instabilities in the lithosphere for various rheological and density structures: Geophysical Journal International, v. 129, p. 95-112.
Danyushevsky, L.V., and P. Plechov, 2011, Petrolog3: Integrated software for modeling crystallization processes: Geochemistry Geophysics Geosystems, v. 12, Q07021.
Dasgupta, R., Hirschmann, M. M., and Smith, N. D., 2007, Partial melting experiments of peridotite + CO_2 at 3 GPa and genesis of alkalic ocean island basalts: Journal of Petrology, v. 48, 2093-2124.
Davis, M. and Kusznir, N., 2004. Depth-dependent lithospheric stretching at rifted continental margins, *in* Karner, G.D. (ed.) Proceedings of NSF Rifted Margins Theoretical Institute, Columbia University Press, New York, p. 92-136.
de Boer, J.Z., 1967, Paleomagnetic study of Mesozoic dike swarms in the Appalachians. Journal of Geophysical Research, v. 72, p. 2237-2250.
Defant, M.J., and Drummond, M.S., 1990, Derivation of some modern arc magmas by melting of young subducted lithosphere, Nature, v. 347, p. 662–665.
Defant, M.J., and Drummond, M.S., 1993, Mount St. Helens: Potential example of the partial melting of the subducted lithosphere in a volcanic arc, Geology, v. 21, p. 547-550, doi: 10.1130/0091-7613(1993)021<0547:MSHPEO>2.3.CO;2.
Driscoll, N.W. and Karner, G.D., 1998, Lower crustal extension across the northern Carnarvon Basin, Australia: evidence for an eastward dipping detachment: Journal of Geophysical Research, v. 103, p. 4975-4992.
Dumoulin, C., Doin, M.P., Arcay, D., and Fleitout, L., 2005, Onset of small-scale instabilities at the base of the lithosphere: scaling laws and role of pre-existing lithospheric structures: Geophysical Journal International, v. 160, p. 345-357.
Eby, G.N., 1987, The Monteregian Hills and White Mountain alkaline igneous provinces, eastern North America. In Fitton, J.G. and Upton, B.G.J. (eds.) Alkaline Igneous Rocks, Geological Society Special Publication No. 30. Blackwell Scientific Publications, Oxford, England, pp. 433-447.
Eldholm, O., Gladczenko, T.P, Skogseid, J., and Planke, S., 2000, Atlantic volcanic margins: a comparative study. In: Nøttvedt, A., Larsen, B.T., Olaussen, S., Tørudbakken, B., Skogseid, J., Gabrielsen, R.H., Brekke, H. and Ø. Birkeland (eds.), Dynamics of the Norwegian Margin. Geological Society of London, Special Publication, v. 167, p. 411-428.

936 Elkins-Tanton, L.T., 2005, Continental magmatism caused by lithospheric
937 delamination. In: G.R. Foulger, J.H. Natland, D.C. Presnall, D.L. Anderson,
938 (eds.), Plates, Plumes, and Paradigms, Geological Society of America Special
939 Paper, v. 388, p. 449-461.
940 Elkins-Tanton, L.T., 2007, Continental magmatism, volatile recycling, and a
941 heterogeneous mantle caused by lithospheric gravitational instabilities, Journal
942 of Geophysical Research, v. 112, DOI: 10.1029/2005JB004072.
943 Elkins-Tanton L.T. and T.L. Grove, 2003, Evidence for deep melting of hydrous,
944 metasomatized mantle: Pliocene high potassium magmas from the Sierra
945 Nevadas, Journal of Geophysical Research, v. 108, 2350,
946 DOI: 10.1029/2002JB002168.
947 Esedo, R., van Wijk, J., Coblentz, D., and Meyer, R., 2012, Uplift prior to continental
948 breakup: indication for removal of mantle lithosphere?: Geosphere, v. 8, p.
949 1078-1085.
950 Ewart, A., 1982, The mineralogy and petrology of Tertiary-Recent orogenic volcanic
951 rocks: with special reference to the andesitic-basaltic compositional range; p.
952 25-95 in, Thorp, R.S., ed., Andesites: Orogenic Andesites and Related Rocks,
953 John Wiley and Sons, New York, 724 p.
954 Foulger, G.R., and Anderson D.L., 2005, A cool model for the Iceland hotspot:
955 Journal of Volcanology and Geothermal Research, v. 141, p. 1-22.
956 Furman, T., Kaleta, K.M., Bryce, J.G., and Hanan, B.B., 2006, Tertiary mafic lavas of
957 Turkana, Kenya: Constraints on East African Plume structure and the
958 occurrence of high-μ volcanism in Africa: Journal of Petrology, v. 47, p. 1221-
959 1244, doi: 10.1093/petrology/egl009.
960 Göğüş, O.H., and Pysklywec, R.N., 2008, Near-surface diagnostics of dripping or
961 delaminating lithosphere: Journal of Geophysical Research, v. 113, B11404,
962 doi:10.1029/2007JB005123.
963 Griffin, W.L., O'Reilly, S.Y., Doyle, B.J., Pearson, N.J., Coopersmith, H., Kivi, K,
964 Malkovets, V. and Pokhilenko, N.V., 2004, Lithosphere mapping beneath the
965 North American Plate: Lithos, v. 77, p. 873-902.
966 Grossman, J.N., Gottfried, D., and Froelich, A.J., 1991, Geochemical data for Jurassic
967 diabase associated with Early Mesozoic basins in the eastern United States:
968 USGS Open-File Report, 91-322-J.
969 Haaga, K.A., 2014, Petrogenesis of Jan Mayen Ridge magmas in space and time.
970 University of Bergen. Master of Science thesis in Geochemistry and Petrology.
971 194 p.
972 Hames, W.E. , McHone, J.G., Renne, R., Ruppel, C., 2003, Introduction, In: Hames,
973 W.E., McHone, J. G., Renne, and R. R., Ruppel, C., (eds.) The Central Atlantic
974 Magmatic Province. Insights from fragments of Pangea, Geophysical
975 Monograph, v. 136, p. 1-6.
976 Harry, D.L., and Sawyer, D.S., 1999, A dynamic model of lithospheric extension in
977 the Baltimore Canyon Trough region: Tectonics, v. 11, p. 420-436.
978 Hastie, A.R., Kerr, A.C., Pearce, J.A., and Mitchell, S.F., 2007, Classification of
979 altered volcanic island arc rocks using immobile trace elements: development of
980 the Th-Co discrimination diagram: Journal of Petrology, v. 48, p. 2341-2357.
981 Herzberg, C., 2006, Petrology and thermal structure of the Hawaiian plume from
982 Mauna Kea volcano: Nature, v. 444, p. 605-609.
983 Hibbard, J., van Staal, C., Rankin, D., and Williams, H., 2006, Geology, Lithotectonic
984 Map of the Appalachian Orogen (South), Canada-United States of America.
985 Geological Survey of Canada, Map 02096A, scale 1:1500000.

Houseman, G.A., and Molnar, P., 1997, Gravitational (Rayleigh-Taylor) instability of a layer with non-linear viscosity and convective thinning of continental lithosphere: Geophysical Journal International, v. 128, p. 125–150.

Houseman, G.A., McKenzie, D.P., and Molnar, P., 1981, Convective instability of a thickened boundary-layer and its relevance for the thermal evolution of continental convergent belts: Journal of Geophysical Research, v. 86, p. 6115–6132.

Huang, J., Zhong, S., and van Hunen, J., 2003, Controls on sublithospheric small-scale convection: Journal of Geophysical Research, v. 108, NO. B8, 2405, doi:10.1029/2003JB002456.

Iddings, J.P., 1895, Absarokite – shoshonite – banakite series, The Journal of Geology, v. 3, p. 935 – 959.

Jaeger, J. C., and N.G.W. Cook, 1979, Fundamentals of Rock Mechanics, 593 pp., Chapman and Hall, London.

Johnson, R.W., Milton, C., and Dennison, J.M., 1971, Field trip to the igneous rocks of Augusta, Rockingham, Highland, and Bath Counties, Virginia: Virginia Division of Mineral Resources, Information Circular 16, 68 p.

Joplin, G.A., 1965, The problem of the potash-rich basaltic rocks: Mineralogical Magazine, v. 34, p. 266–275.

Joplin, G.A., 1968, The shoshonite association: a review: Journal of the Geological Society of Australia, v. 15, p. 275–294.

Kay, R.W., 1978, Aleutian magnesian andesites: melts from subducted Pacific Ocean crust. Journal of Volcanology and Geothermal Research, v. 4, p. 117-132.

Kay, R.W., Mahlburg Kay, S., 1993, Delamination and delamination magmatism: Tectonophysics, v. 219, p. 177-189.

Kay, R.W., and Mahlburg Kay, S., 2002, Andean adakites: three ways to make them: Acta Petrologica Sinica, v. 18, p. 303-311.

King, S.D., and Anderson, D.L., 1998, Edge-driven convection: Earth and Planetary Science Letters, v. 160, p. 289-296.

Korenaga, J., 2004, Mantle mixing and continental breakup magmatism: Earth and Planetary Science Letters, v. 218, p. 468-473.

Kruse, S., McNutt, M., Phipps-Morgan, J., and Royden, L., 1991, Lithospheric extension near Lake Mead, Nevada: a model for ductile flow in the lower crust: Journal of Geophysical Research, v. 96, p. 4435-4456.

Kusznir, J.J. and Karner, G.D., 2007, Continental lithospheric thinning and breakup in response to upwelling divergent mantle flow: application to the Woodlark, Newfoundland and Iberia margins: Geological Society Special Publication, v. 282, p. 389-419.

Levander, A., Schmandt, B., Miller, M.S., Liu, K., Karlstrom, K., Crow, R., Lee, C.T., Humphreys, E., 2011, Continuing Colorado Plateau uplift by delamination-style convective lithospheric downwelling: Nature, v. 472, p. 461-465, doi:10.1038/nature10001.

Lustrino, M., 2005, How the delamination and detachment of lower crust can influence basaltic magmatism: Earth-Science Reviews, v. 72, p. 21-38.

Mallik, A., and Dasgupta, R., 2013, Reactive infiltration of MORB-eclogite-derived carbonated silicate melt into fertile peridotite at 3 GPa and genesis of alkalic magmas: Journal of Petrology, v. 54, p. 2267-2300.

Mallik, A., and Dasgupta, R., 2014, Effect of variable CO_2 on eclogite-derived andesite-lherzolite reaction at 3 GPa - Implications for mantle source

characteristics of alkalic ocean island basalts: Geochemistry, Geophysics, Geosystems, v. 15, p. 1533-1557.
Martin, H., 1999, Adakitic magmas: modern analogues of Archean granitoids: Lithos, v. 46, p. 411-429, DOI: 10.1016/S0024-4937(98)00076-0.
Martin, H., Smithies, R.H., Rapp, R., Moyen, J.-F., and Champion, D., 2005, An overview of adakite, tonalite–trondhjemite–granodiorite (TTG), and sanukitoid: relationships and some implications for crustal evolution, Lithos, v. 79, p. 1–24.
Martins, L.T., Madeira, J., Youbi, N., Munhá, J., Mata, J., and Kerrich, R., 2008, Rift-related magmatism of the Central Atlantic magmatic province in Algarve, Southern Portugal: Lithos, v. 101, p. 102-124, doi:10.1016/j.lithos.2007.07.010.
Marvin, R.F., 1968, Transcontinental geophysical survey (35°-39° N), radiometric age determinations of rocks: U.S. Geological Survey Map I-537.
Marzoli, A., Renne, P.R., Piccirillo, E.M., Ernesto, M.; Bellieni, G., De Min, A., 1999, Extensive 200 million-year-old continental flood basalts of the central Atlantic magmatic province: Science, v. 284, p. 616–618.
Marzoli, A., Jourdan F., Puffer, J.H., Cupone, T., Tanner, L. H., Weems, R.E., Bertrand, H., Cirilli, S., Bellieni, G., and De Min, A., 2011, Timing and duration of the Central Atlantic magmatic province in the Newark and Culpeper basins, eastern U.S.A.: Lithos, v. 122, p. 175-188.
Matton, G., Jébrak, M., 2009, The Cretaceous Peri-Atlantic Alkaline Pulse (PAAP): Deep mantle plume origin or shallow lithospheric breakup?: Tectonophysics, v. 469, p. 1-12, doi:10.1016/j.tecto.2009.01.001.
Mazza, S., Gazel, E., Johnson, E.A., McAleer, R., Kunk, M., Spotila, J., Bizimis, M., and Coleman, D., 2014, Volcanoes of the passive margin: the youngest magmatic event in Eastern North America: Geology, v. 42, p. 483-486, doi: 10.1130/G35407.1.
McHone, J.G., 1996, Broad-terrane Jurassic flood basalts across northeastern North America: Geology, v. 24, p. 319-322.
McKenzie, D., 1978, Some remarks on the development of sedimentary basins: Earth and Planetary Science Letters, v. 40, p. 25-32.
McKenzie, D., and M.J. Bickle, 1988, The volume and composition of melt generated by extension of the lithosphere: Journal of Petrology, v. 29, p. 625-679.
Merle, R., Marzoli, A., Reisberg, L., Bertrand, H., Nemchin, A., Chiaradia, M., Callegaro, S., et al., 2014, Sr, Nd, Pb and Os Isotope Systematics of CAMP Tholeiites from Eastern North America (ENA): Evidence of a Subduction-enriched Mantle Source: Journal of Petrology, v. 55, p. 133-180.
Meyer, R., Schultz, L., Hendriks, B.W., Harbor, D. J., Connors, C.D., 2011, Central Appalachian Valley and Ridge Province Cenozoic igneous activity and its relation in space and time with the Late Jurassic rift-to-drift-related alkalic dikes: American Geophysical Union, Fall Meeting 2011, abstract #T24A-04.
Meyer, R., Hertogen, J.G.H., Pedersen, R.B., Viereck-Götte, L., and Abratis, M., 2009, Interaction of mantle derived melts with crust during the emplacement of the Vøring Plateau, N.E. Atlantic: Marine Geology, v. 261, p. 3-16.
Meyer, R., van Wijk, J. and Gernigon, L., 2007, North Atlantic Igneous Province: a review of models for its formation. In: Foulger, G.R. and Jurdy, D.M. (eds.), The Origins of Melting Anomalies: Plates, Plumes and Planetary Processes. Geological Society of America Special Paper, v. 430, p. 525-552.
Meyer, R., Abratis, M., Viereck-Götte, L., Mädler, J., Hertogen, J., and Romer, R.L., 2002, Mantelquellen des Vulkanismus in der thüringischen Rhön. Beiträge zur Geologie von Thüringen. N.F. v. 9, p. 75-105.

1085 Meyer, H.O.A., 1976, Kimberlites of the Continental United States: A Review: The
1086 Journal of Geology, v. 84, 377-403.
1087 Moresi, L.N., Dufour, F., and Mühlhaus, H., 2003, A Lagrangian integration point
1088 finite element method for large deformation modeling of viscoelastic
1089 geomaterials: Journal of Computational Physics, v. 184, p. 476-497.
1090 Moresi, L., and Gurnis, M., 1996, Constraints on the lateral strength of slabs from
1091 three-dimensional dynamic flow models: Earth and Planetary Science Letters, v.
1092 138, p. 15-28.
1093 Nelson, K.D., 1992, Are crustal thickness variations in old mountain belts like the
1094 Appalachians a consequence of lithospheric delamination?: Geology, v. 20, p.
1095 482-502.
1096 Pegram, W. J., 1990, Development of continental lithospheric mantle as reflected in
1097 the chemistry of the Mesozoic Appalachian tholeiites. U.S.A: Earth and
1098 Planetary Science Letters, v. 97, p. 316-331.
1099 Peron-Pinvidic, G., Shillington, D.J., and Tucholke, B.E., 2010, Characterization of
1100 sills associated with the U reflection on the Newfoundland margin: evidence
1101 for widespread early post-rift magmatism on a magma-poor rifted margin:
1102 Geophysical Journal International, v. 182, p. 113-136, doi: 10.1111/j.1365-
1103 246X.2010.04635.x.
1104 Puffer, J.H., 2003, A reactivated back-arc source for CAMP magma: in Hames, W.E.,
1105 McHone, J.G., Renne, P.R., and Ruppel, C. (editors), The Central Atlantic
1106 Magmatic Province: Insights from Fragments of Pangea: American Geophysical
1107 Union Geophysical Monograph 136, p. 151-162.
1108 Ragland, P.C., Cummins, L.E., and Arthur, J.D., 1992, Compositional patterns for
1109 early Mesozoic diabases from South Carolina to central Virginia: Geological
1110 Society of America Special Paper, v. 268, p. 309-332, doi:10.1130/SPE-268-
1111 p309.
1112 Rapp, R.P., and Watson, E.B., 1995, Dehydration melting of metabasalt at 8–32 kbar:
1113 Implications for continental growth and crust-mantle recycling: Journal of
1114 Petrology, v. 36, p. 891-931, doi: 10.1093/petrology/36.4.891.
1115 Rapp, R.P., Shimizu, N., Norman, M.D. and Applegate, G.S., 1999, Reaction between
1116 slab-derived melts and peridotite in the mantle wedge: experimental constraints
1117 at 3.8 GPa: Chemical Geology, v. 160, p. 335–356.
1118 Raymond, L.A., Swanson, S., Love, A., and Allan, J., 2003, Cr-spinel compositions,
1119 metadunite petrology, and the petrotectonic history of Blue Ridge ophiolites,
1120 Southern Appalachian Orogen, USA: Geological Society, London, Special
1121 Publications, v. 218, p. 253-278, doi: 10.1144/GSL.SP.2003.218.01.14.
1122 Rudnick, R.L., and Gao, S., 2003, Composition of the continental crust. In *The Crust*,
1123 vol. 3 (ed. R. L. Rudnick). Elsevier, pp. 1-64.
1124 Sacks, P.E., Secor Jr., D.T., 1990, Delamination in collisional orogens: Geology, v.
1125 18, p. 999-1002.
1126 Saleeby J., Ducea M., and Clemens-Knott D., 2003, Production and loss of high-
1127 density batholithic root, southern Sierra Nevada, California: Tectonics, v. 22,
1128 doi:10.1029/2002TC001374.
1129 Saleeby J., and Foster Z., 2004, Topographic response to mantle lithosphere removal
1130 in the southern Sierra Nevada region: Geology, v. 32, p. 245-248.
1131 Saleeby J., Le Pourhiet L., Saleeby Z., and Gurnis M., 2012, Epeirogenic transients
1132 related to mantle lithosphere removal in the southern Sierra Nevada region,
1133 California, part I: Implications of thermomechanical modeling: Geosphere, v. 8,
1134 p. 1286-1309.

1135 Saleeby J., Saleeby Z., and Le Pourhiet L., 2013, Epeirogenic transients related to
1136 mantle lithosphere removal in the southern Sierra Nevada region, California:
1137 Part II. Implications of rock uplift and basin subsidence relations: Geosphere, v.
1138 9, p. 394-425.
1139 Salters, V.J.M., Ragland, P.C., Hames, W.E., Mila, K., and Ruppel, C., 2003,
1140 Temporal chemical variations within lowermost Jurassic tholeiite magmas of
1141 the Central Atlantic Magmatic Province, In Hames, W.E., McHone, J.G.,
1142 Renne, P.R., and Ruppel, C., (eds.), The Central Atlantic Magmatic Province:
1143 American Geophysical Union, Geophysical Monograph, v. 136, p. 163-178.
1144 Schlische, R.W., and Withjack, M.O., 2003, Relative timing of CAMP, rifting,
1145 continental breakup, and basin inversion: tectonic significance, In: Hames,
1146 W.E., McHone, J. G., Renne, and R. R., Ruppel, C., (eds.) The Central Atlantic
1147 Magmatic Province. Insights from fragments of Pangea, Geophysical
1148 Monograph, v. 136, p. 33-59.
1149 Schmincke, H.U., 2007, The Quaternary volcanic fields of the east and west Eifel
1150 (Germany), Mantle plumes, Springer, p. 241-322.
1151 Shaw, D.M., 2006, Trace Elements in Magmas – A Theoretical Treatment,
1152 Cambridge University Press, Cambridge, 243 pp.
1153 Sinha, A.K., Thomas, W.A., Hatcher Jr., R.D., Harrison, T.M., 2012, Geodynamic
1154 evolution of the central Appalachian orogeny: Geochronology and
1155 compositional diversity of magmatism from Ordovician through Devonian:
1156 American Journal of Science, v. 312, p. 907-966.
1157 Sleep, N.H., 2007, Edge-modulated stagnant-lid convection and volcanic passive
1158 margins: Geochemistry Geophysics Geosystems, v. 8, no. 12, Q12004.
1159 Smithies, R.H., 2000, The Archaean tonalite-trondhjemite-granodiorite (TTG) series
1160 is not an analogue of Cenozoic adakite: Earth and Planetary Science Letters, v.
1161 182, p. 115-125.
1162 Sun, S.S. and McDonough, W.F., 1989, Chemical and isotopic systematics of oceanic
1163 basalts; implications for mantle composition and processes. In: Magmatism in
1164 the ocean basins. Saunders, A.D. and Norry, M.J. (Editors), Geological Society
1165 of London, London, v. 42, p. 313-345.
1166 Turcotte, D. L., and G. Schubert, 2002, Geodynamics, Cambridge Univ. Press, New
1167 York, pp. 472.
1168 van Hunen, J., and Allen, M.B., 2011, Continental collision and slab break-off: A
1169 comparison of 3-D numerical models with observations: Earth and Planetary
1170 Science Letters, v. 302, p. 27–37, doi:10.1016/j.epsl.2010.11.035.
1171 van Hunen, J.S., Zhong, S., Shapiro, N.M., and Ritzwoller, M.H., 2005, New
1172 evidence for dislocation creep from 3-D geodynamic modeling of the Pacific
1173 upper mantle structure: Earth and Planetary Science Letters, v. 238, p. 146-155,
1174 doi:10.1016/j.epsl.2005.07.006.
1175 van Wijk, J., Baldridge, S., van Hunen, J., Goes, S., Aster, R., Coblentz, D., Grand,
1176 S., and Ni, J., 2010, Small-scale convection at the edge of the Colorado Plateau:
1177 implications for topography, magmatism, and evolution of Proterozoic
1178 lithosphere: Geology, v. 38, p. 611-614, doi: 10.1130/G31031.1.
1179 Walter, M.J., 1998, Melting of garnet peridotite and the origin of komatiite and
1180 depleted lithosphere: Journal of Petrology, v. 39, p. 29–60.
1181 Wang, Y., Forsyth, D., Ray, C., Carriero, N., Schmandt, B., Gaherty, J., and Savage,
1182 B., 2013, Fossil slabs attached to unsubducted fragments of the Farallon plate:
1183 Proceedings of the National Academy of Sciences of the United States of
1184 America, v. 110, p. 5342–5346, doi: 10.1073/pnas.1214880110.

Wang, P., and Glover, III L., 1997, The mafic-ultramafic association in the Virginia Blue Ridge cover rocks: Rifting sequence or ophiolitic mélange? In: Glover, III L., and Gates, A.E. (eds.) Central and Southern Appalachian sutures: results of the EDGE Project and related studies: Geological Society of America Special Papers, v. 314, p. 65-87.

Wang, Q., McDermott, F., Xu, J., Bellon, H., Zhu, Y., 2005, Cenozoic K-rich adakitic volcanic rocks in the Hohxil area, northern Tibet: lower-crustal melting in an intracontinental setting: Geology, v. 33, p. 465-468.

Willbold, M., and Stracke, A., 2010, Formation of enriched mantle components by recycling of upper and lower continental crust: Chemical Geology, v. 276, p. 188–197.

Watson, T.L., and Cline, J.H., 1913, Petrology of a series of igneous dikes in central western Virginia. Geological Society of America Bulletin, v. 24, p. 301–334.

Xu, J.F., Shinjio, R., Defant, M.J., Wang, Q., and Rapp, R.P., 2002, Origin of Mesozoic adakitic intrusive rocks in the Ningzhen area of east China: Partial melting of delaminated lower continental crust?: Geology, v. 30, p. 1111-1114.

Yogodzinski, G.M., Kay, R.W., Volynets, O.N., Koloskov, A.V., and Kay, S.M., 1995, Magnesian andesite in the western Aleutian Komandorsky region: Implications for slab melting and processes in the mantle wedge: Geological Society of America Bulletin, v. 107, no. 5, p. 505-519.

Yuan, H., Romanowicz, B., 2010, Lithospheric layering in the North American craton: Nature, v. 466, p. 1063-1069.

Zandt, G., Gilbert, H., Owens, T.J., Ducea, M., Saleeby, J., and Jones, C., 2004, Active foundering of a continental arc root beneath the southern Sierra Nevada in California: Nature, v. 431, p. 41-46.

Zartman, R.E., Brock, M.R., Heyl, A.V., and Thomas, H.H., 1967, K-Ar and Rb-Sr ages of some alkaline intrusive rocks from central and eastern United States: American Journal of Science, v. 265, p. 848–870.

Zhong, S., Zuber, M.T., Moresi, L., and Gurnis M., 2000, Role of temperature-dependent viscosity and surface plates in spherical shell models of mantle convection: Journal of Geophysical Research, v. 105, p. 11063-11082.

Figure captions

Figure 1a: Southeastern U.S. Central Atlantic Magmatic Province (CAMP) dyke swarm compilation map from Ragland et al. (1983). The dykes studied here (light grey square) have been mapped as CAMP in e.g. Callegaro et al. (2013), Beutel et al., (2005), Hames et al., (2003), Hames and Renne (2000), and Ragland et al., (1992).

Figure 1b: Tectonic sketch map of Virginia, USA, illustrating its different physiographic regions (lower panel). The study area is indicated by the black box. Upper panel: West-Central Virginian study area with the distribution of igneous rocks and dykes and the sample locations of high-Si (blue) and low-Si adakites (red). For orientation, the cities of Staunton and Harrisonburg are indicated in black. Yellow triangle indicates the kimberlite of Mt. Horeb; Lynchburg is the type locality of the Lynchburg formation (red circle). Younger (50 Ma) igneous outcrops in West Virginia are only plotted for reference (Meyer et al. 2011). Map modified after Johnson et al. (1971).

Figure 2: Classification of subalkalic rocks in the K_2O vs. SiO_2 diagram (Ewart, 1982). The diagram classifies the excessive high-K magmas as bi-modal shoshonitic

alkaline series. Red samples are the low-Si adakitic rocks, blue samples are high-Si adakitic rocks. Grey samples are all CAMP samples within the CAMP dataset from the Max Planck Institute for Chemistry maintained GEOROC (Geochemistry of Rocks of the Oceans and Continents) database (http://georoc.mpch-mainz.gwdg.de/georoc/).

Figure 3: Th and Co are not fractionated during post-magmatic processes. The geochemical variation of these elements is used to confirm the volcanic-arc-like K-rich magmatic nature of the studied rocks (diagram after Hastie et al., 2007; red samples are the low-Si adakitic rocks, blue samples are high-Si adakitic rocks). Grey samples are all CAMP samples with a K_2O content > 1 wt. % within the CAMP dataset from the GEOROC database (http://georoc.mpch-mainz.gwdg.de/georoc/).

Figure 4: Classical adakitic Sr/Y versus Y plot for the Virginia igneous rocks sample set. Adakite fields (grey, purple, black-dashed) are from Martin (1999). Melting curves: green melting curves are from Drummond and Defant (1990; tick marks indicate melting degrees); orange melting curve from Castillo (2008) of 50% amphibole, 45% phlogopite and 5% garnet. Source materials: (1) MORB-type eclogite (with 141 ppm Sr and 21 ppm Y) (2) MORB-type amphibolite (with 264 ppm Sr and 38 ppm Y). Melting of amphibolites can reproduce the observed geochemistry of the high-K, high-Si igneous rocks in Virginia. Red samples are low-Si adakitic rocks, blue samples are high-Si adakitic rocks.

Figure 5: Comparison between the observed high-Si adakites and our model curves for non-modal batch melting of a continental arc lower crustal lithology (Rudnick and Gao, 2003) with a modal composition of (60 wt.%) amphibole + (35 wt.%) clinopyroxene + (10 wt. %) garnet + (accessory) magnetite + apatite. This modal composition is close to reported amphibolitic lithologies within the Lynchbourg formation. A best fit between the measured data (blue) and the orange modal composition is achieved for a partial melting degree of 10%. VA is Virginia.

Figure 6: C1-normalized REE plots for the Jurassic high-K rich magmas in Virginia and modeled melt compositions. The high-Si magmas have a distinct U-shape REE pattern reflecting the amphibole source and their partition coefficients. The HREE contents point towards garnet as a residual phase in the source. The low-Si magmas cannot be produced by a REE-primitive or depleted mantle. Their lherzolite source must have been metasomatized. Simple batch melting calculations (dashed lines) suggest that 5 to 10% of melting from a spinel-lherzolite source that has been preconditioned with fluids and melts from a dehydrating garnet bearing rock can produce the observed REE patterns. Easter North America CAMP tholeiites are shown for comparison (Merle et al., 2013). (Normalizing data from Sun and McDonough, 1989).

Figure 7: Possible source rocks and potential melt evolution trends for the K-rich melts from central Virginia. CaO vs. SiO_2 petrological discrimination diagram between CO_2-saturated and deficient melts from Herzberg and Asimow (2008) for magmas produced in the garnet stability field (ca. 3 GPa). The diagonal line separates magmas from a carbonated peridotite from melts produced by a “fresh” garnet peridotite. The high SiO_2 magmas reflect their adakite petrogenesis with similarities to experimental melts produced from meta-basalt melting. In contrast, the low SiO_2

samples have similarities to andesitic melts interacting with garnet bearing peridotite. Some samples have also the characteristics of the dry parental melts of a garnet peridotite. However, the Petrolog (http://petrolog.web.ru) modeled liquid line of descent (LLD) follows a different path from the studied samples.

Figure 8: Models for lithosphere instabilities below rift margins. Color scale is temperature, flow field of the mantle is indicated by arrows. The 410 km phase transition is indicated by a black dashed line. A) Continental rift stage. Mantle flow 7 Myr after rifting initiated. Small-scale convection cells start to develop in the rift. B) Early breakup-stage, 9.5 Myr after rifting started. Instabilities start to develop below the margins of the rift. Small-scale convection in the rift zone is well developed. I indicates possible location of melting of the instability (see discussion in text). C) The instabilities migrate continent-ward with ongoing extension. Sinking of the instabilities below the 410 km phase transition creates a counter flow that brings transition zone material up into the rift and below the margins. "ddt" indicates the area where "depth-dependent thinning" (Driscoll and Karner, 1998; Kusznir and Karner, 2007) occurs. This is an area where more than a proportional amount of mantle lithosphere material is removed from the lithosphere, resulting in margin uplift.

Figure 9: Model results showing the onset of delamination following the development of a gravitational instability below a margin. A) Setup of the geodynamic model. The lithosphere is rheologically layered (see text) into a brittle upper crust (light blue), viscous lower crust (light pink), lithospheric mantle (dark pink) and sub-lithospheric mantle (dark blue). An instability will form at the margin between the thinned lithosphere (toward the left of the model domain) and un-thinned lithosphere toward the right. Domain of the panels that are shown in B) and C) is indicated by the black stippled box. B) Same color-code as in A). This panel shows the deformed lithosphere and the formation of a lithospheric drip ~10 Myr after the initial setup shown in A). The model predicts a zone of yielding above the drip, indicated by the yellow color. This is interpreted as the onset of delamination of the drip. The black dashed line shows the initial lithosphere-asthenosphere boundary. C) Horizontal deviatoric stresses at the same timestep as shown in B). Red is extension, blue is compression. The black dashed line shows the initial lithosphere-asthenosphere boundary. A zone of high strain rates corresponds to the yielding zone in B).

Table captions

Table 1: Volatile free major element and LOI concentrations in wt.% of the sampled high- and low-Si adakitic rocks.

Table 2a: Trace element abundances in ppm within the low-Si type adakitic rocks.

Table 2b: Trace element abundances in ppm within the high-Si type adakitic rocks.

Table 3: Comparison between preferred values from GeoReM database (http://georem.mpch-mainz.gwdg.de/) for 3 USGS international standard reference materials (BCR-2, Columbia River Basalt; DNC-1, Braggtown NC. Olivine-normative Dolerite; W-2, Centerville VA. Diabase) and our measurements.

1334 Fig. 1a:

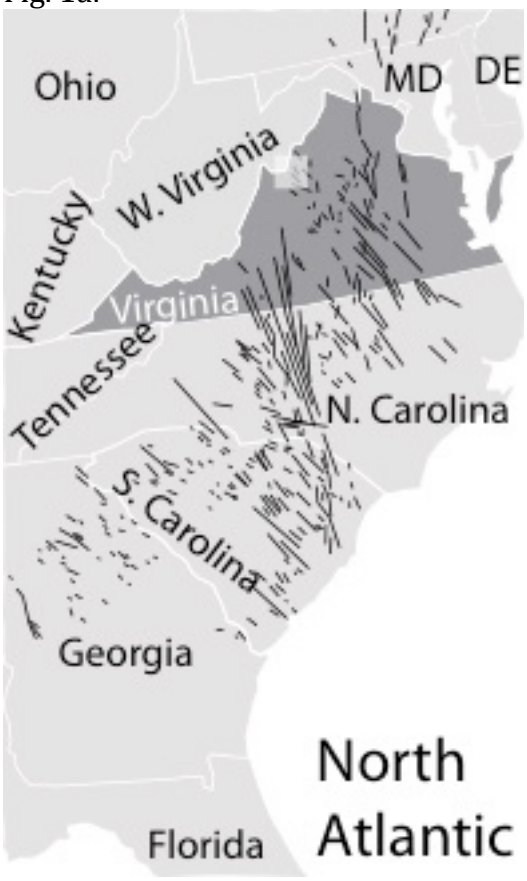

1335
1336

1337 Fig. 1b

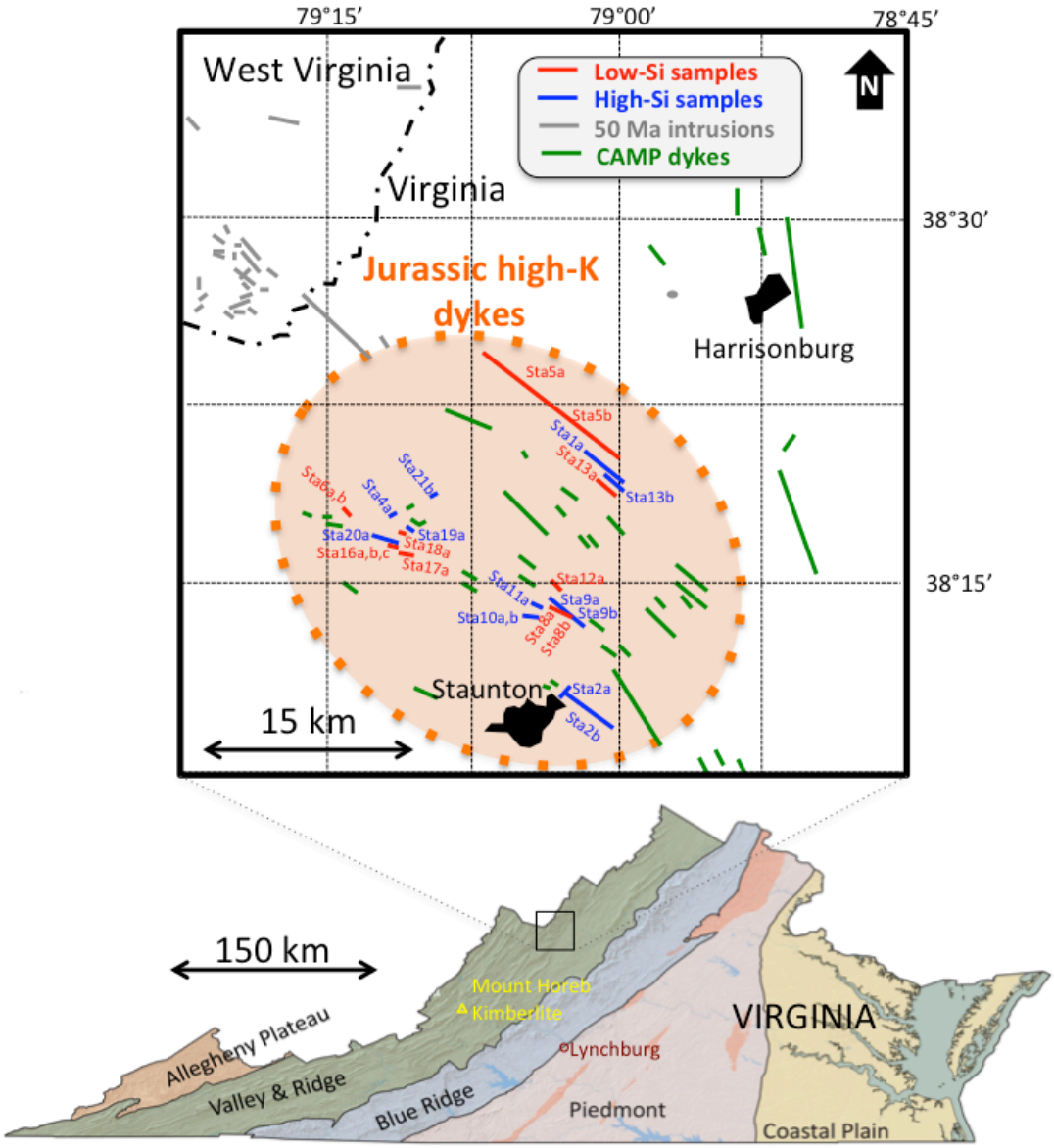

1338
1339

1340 Fig. 2

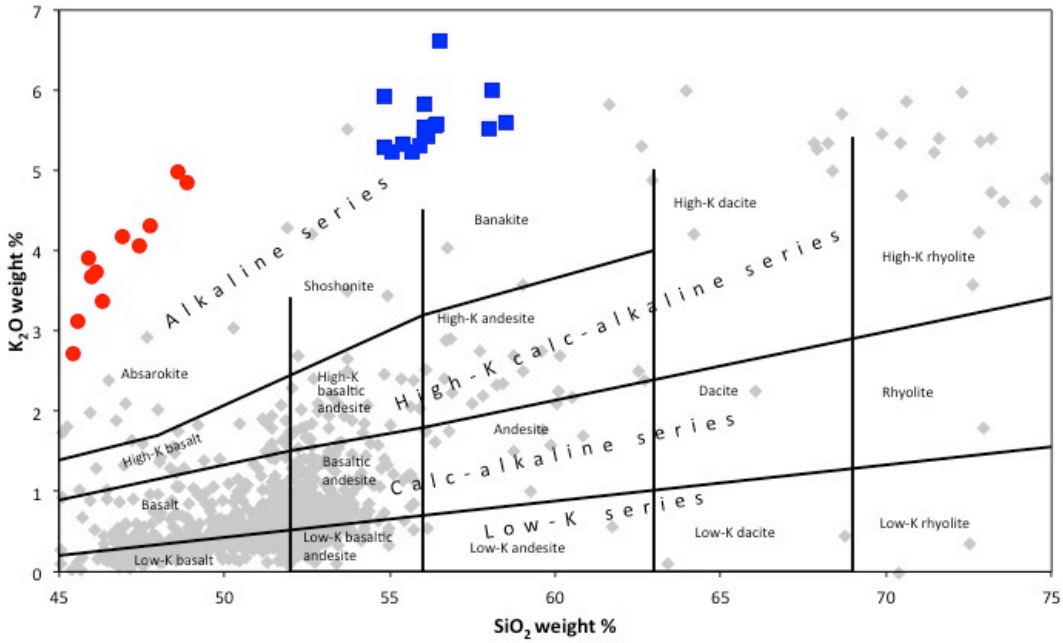

1341
1342 Fig. 3

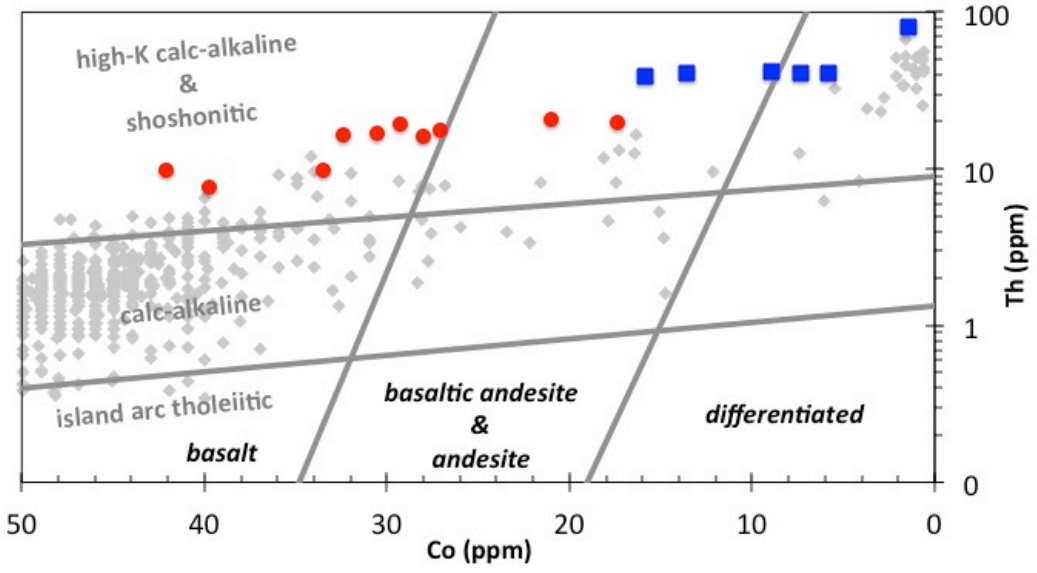

1343
1344
1345
1346

1347 Fig. 4

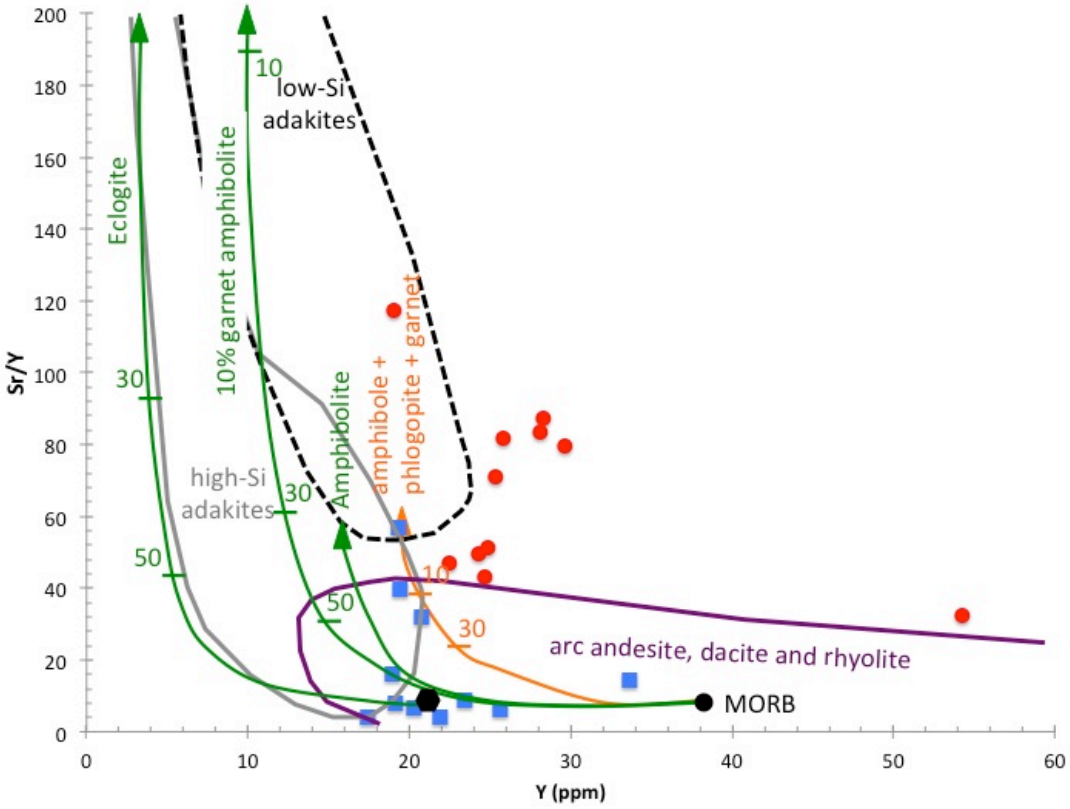

1348
1349 Fig. 5

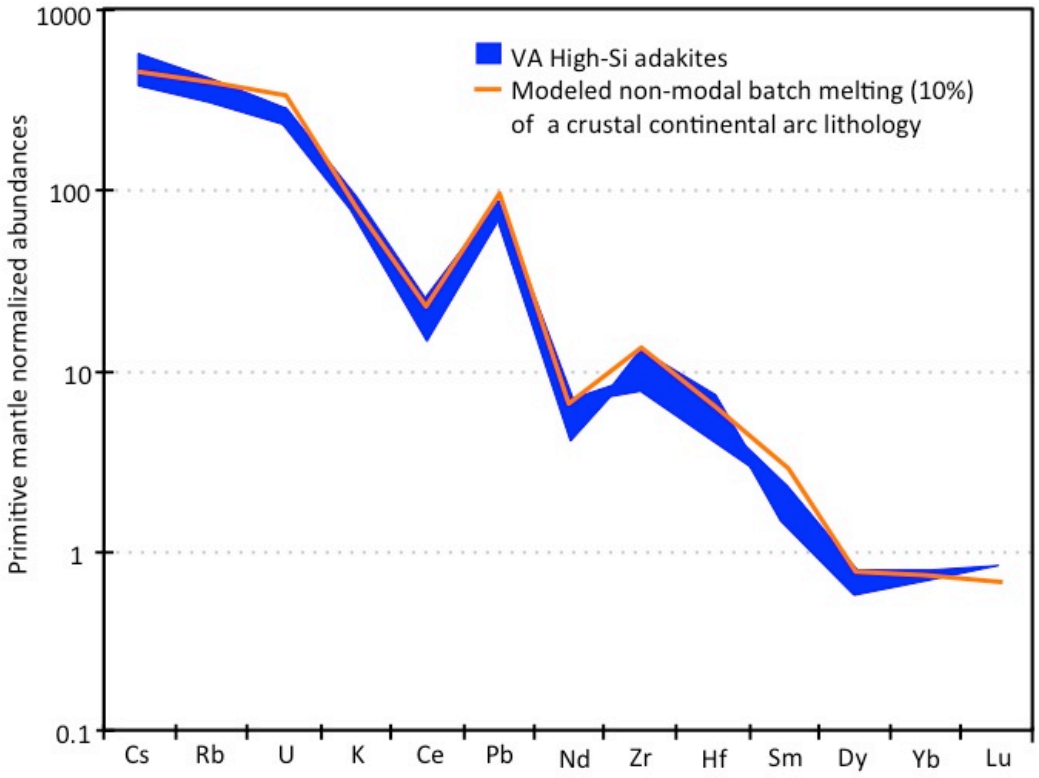

1350
1351
1352
1353

Fig. 6

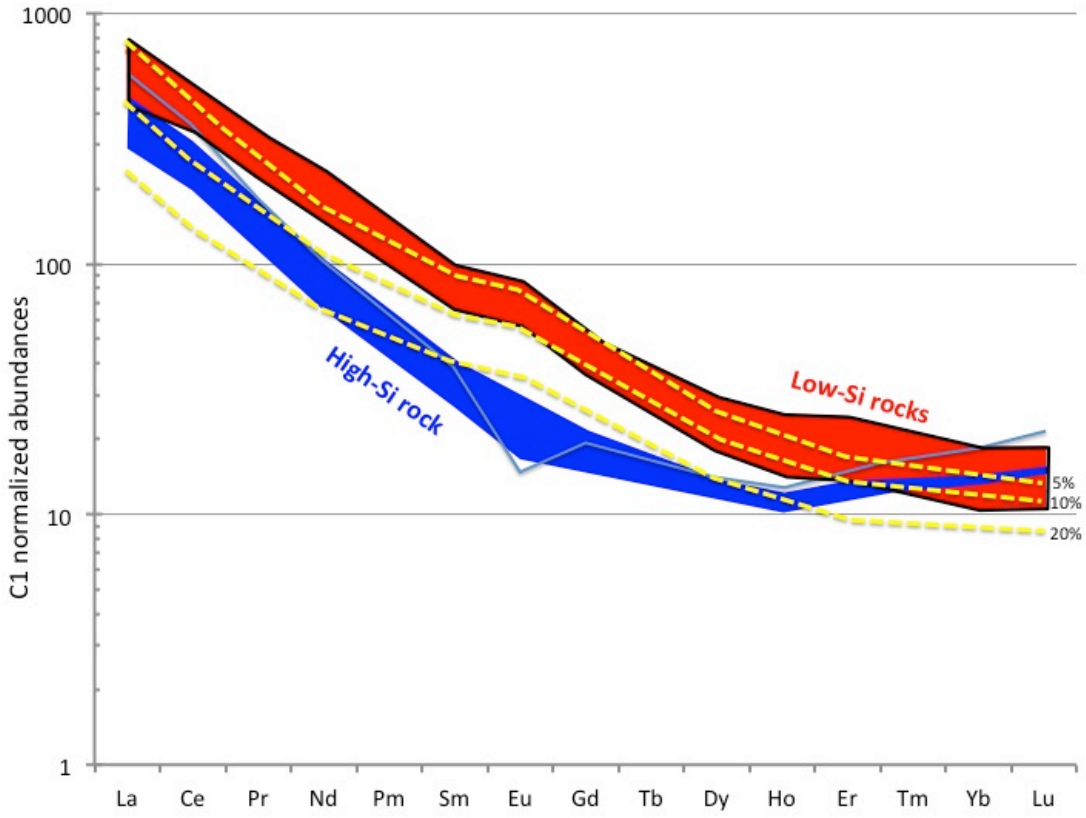
1000
100
10
1
C1 normalized abundances
High-Si rock
Low-Si rocks
5%
10%
20%
La
Ce
Pr
Nd
Pm
Sm
Eu
Gd
Tb
Dy
Ho
Er
Tm
Yb
Lu

Fig. 7

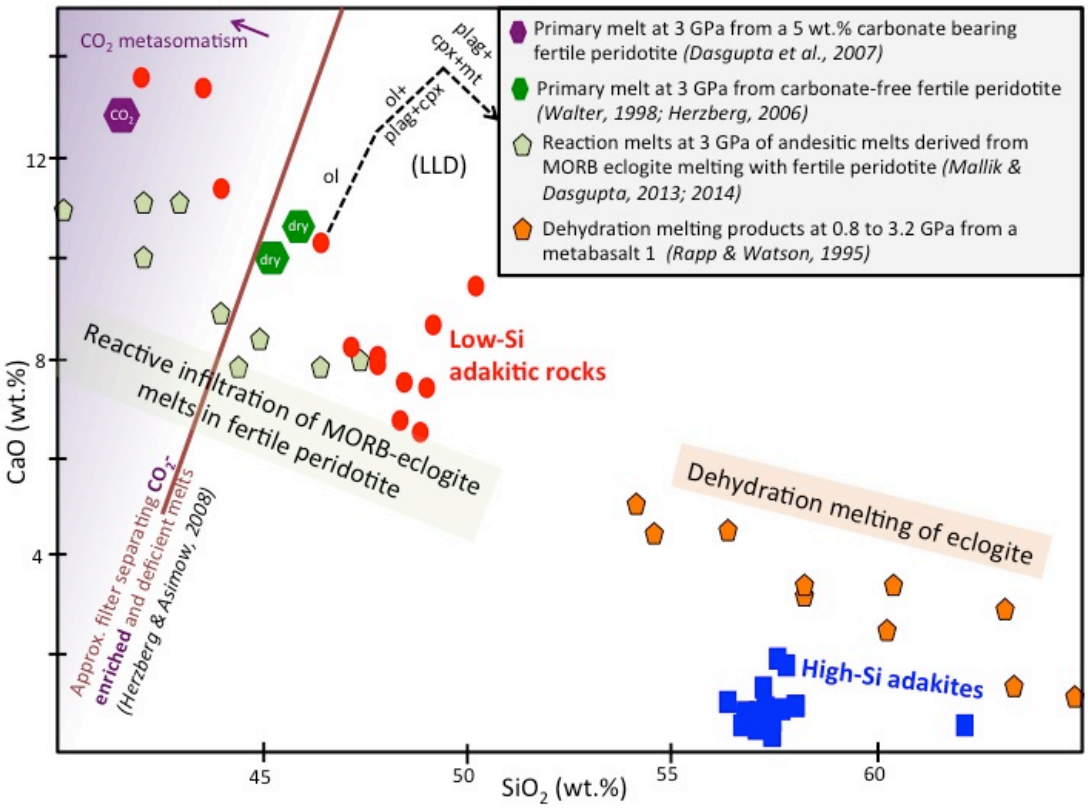
CO2 metasomatism
CO2
dry
dry
ol
ol+
plag+cpx
plag+
cpx+mt
(LLD)
Primary melt at 3 GPa from a 5 wt.% carbonate bearing fertile peridotite (Dasgupta et al., 2007)
Primary melt at 3 GPa from carbonate-free fertile peridotite (Walter, 1998; Herzberg, 2006)
Reaction melts at 3 GPa of andesitic melts derived from MORB eclogite melting with fertile peridotite (Mallik & Dasgupta, 2013; 2014)
Dehydration melting products at 0.8 to 3.2 GPa from a metabasalt 1 (Rapp & Watson, 1995)
Low-Si adakitic rocks
Reactive infiltration of MORB-eclogite melts in fertile peridotite
Dehydration melting of eclogite
High-Si adakites
Approx. filter separating CO2-enriched and deficient melts (Herzberg & Asimow, 2008)
CaO (wt.%)
12
8
4
45
50
55
60
SiO2 (wt.%)

1361 Fig. 8

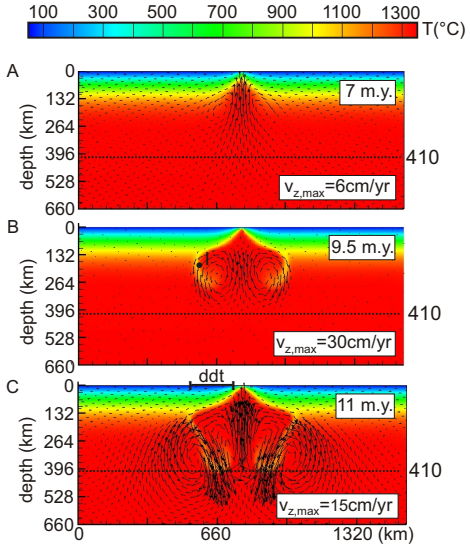

1362
1363
1364
1365
1366
1367
1368
1369
1370
1371
1372

1373 Fig. 9

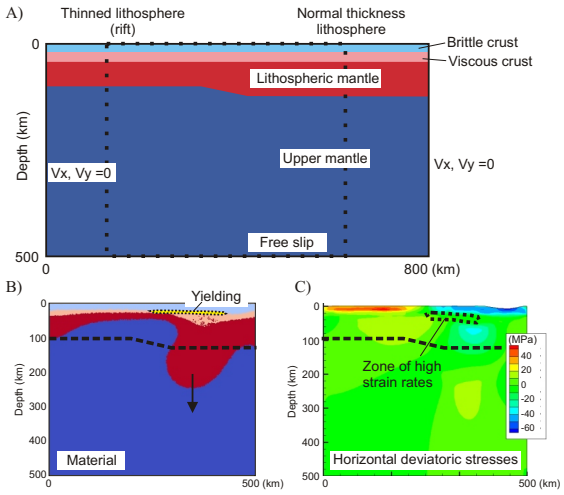

1374
1375

Table 1: Volatile free major element and LOI concentrations in wt.% of the sampled high- and low-Si adakitic rocks.

Type	Sample	SiO_2	TiO_2	Al_2O_3	Cr_2O_3	Fe_2O_3T	MnO	MgO	CaO	Na_2O	K_2O	P_2O_5	LOI
low-Si	Stan18A	41.99	1.95	13.18	0.04	11.65	0.21	9.39	13.59	3.71	3.13	1.15	5.31
low-Si	Stan13A	43.47	2.18	13.53	0.05	10.73	0.19	9.46	13.37	2.71	3.20	1.13	5.53
low-Si	Stan14A	44.04	2.50	15.02	0.01	12.42	0.21	6.87	11.35	3.41	2.86	1.33	3.84
low-Si	Stan06B	47.18	1.68	16.68	n.a.	11.17	0.20	5.26	8.16	5.10	2.82	1.74	n.a.
low-Si	Stan12A	46.49	1.99	16.31	0.02	11.02	0.18	6.45	10.27	2.91	3.18	1.16	5.11
low-Si	Stan05C	48.32	2.02	17.25	n.a.	10.61	0.19	4.12	6.72	5.47	4.12	1.18	4.75
low-Si	Stan17A	47.79	1.55	17.05	0.01	10.40	0.19	4.70	8.02	4.94	3.81	1.53	3.25
low-Si	Stan06A	47.76	1.63	17.00	0.01	10.76	0.20	4.67	7.79	5.08	3.49	1.62	4.75
low-Si	Stan16B	48.34	1.55	17.32	n.a.	10.29	0.19	4.51	7.48	4.44	4.30	1.59	n.a.
low-Si	Stan05A	48.86	2.04	17.36	n.a.	10.56	0.19	3.91	6.47	5.29	4.18	1.14	n.a.
low-Si	Stan16C	48.98	1.35	17.65	n.a.	9.47	0.19	4.10	7.33	5.10	4.42	1.38	n.a.
low-Si	Stan08A	49.16	1.45	17.85	n.a.	9.08	0.15	4.41	8.57	1.10	5.05	1.16	n.a.
low-Si	Stan08B	50.21	1.47	18.28	n.a.	9.12	0.15	4.05	9.43	1.11	4.98	1.18	5.88
high-Si	Stan01A	56.31	0.33	22.92	n.a.	2.39	0.16	0.08	1.04	10.54	6.08	0.12	3.25
high-Si	Stan19A	56.81	0.13	22.23	n.a.	3.54	0.26	0.19	0.77	10.46	5.49	0.11	5.37
high-Si	Stan20A	57.44	0.19	23.37	n.a.	1.84	0.19	0.08	0.33	11.08	5.46	0.02	5.76
high-Si	Stan02B	57.03	0.25	23.00	n.a.	2.62	0.22	0.07	0.45	10.84	5.49	0.04	n.a.
high-Si	Stan04A	56.72	0.09	22.72	n.a.	2.77	0.24	0.01	0.53	11.52	5.33	0.09	n.a.
high-Si	Stan13B	57.27	0.32	23.21	n.a.	2.38	0.15	0.20	1.12	9.80	5.44	0.10	5.07
high-Si	Stan02A	57.20	0.38	21.88	n.a.	3.54	0.22	0.28	1.32	9.41	5.59	0.18	5.12
high-Si	Stan09A	57.49	0.28	22.90	n.a.	2.41	0.17	0.08	0.67	9.92	5.97	0.10	3.88
high-Si	Stan11A	57.57	0.30	22.53	n.a.	2.65	0.17	0.11	0.85	10.01	5.69	0.09	n.a.
high-Si	Stan21B	57.61	0.51	20.28	n.a.	4.52	0.18	0.56	1.83	8.66	5.57	0.27	n.a.
high-Si	Stan10B	57.25	0.29	22.54	n.a.	2.63	0.18	0.22	0.89	10.26	5.65	0.08	n.a.
high-Si	Stan21B	57.66	0.50	20.28	n.a.	4.50	0.18	0.53	1.80	8.58	5.70	0.27	n.a.

high-Si	Stan09B	57.99	0.35	22.30	n.a.	2.94	0.18	0.13	0.96	8.25	6.78	0.11	n.a.
high-Si	Stan10A	57.04	0.30	22.52	n.a.	2.65	0.20	0.08	0.80	10.43	5.90	0.10	3.73
high-Si	Stan07A	57.35	0.18	23.43	n.a.	1.75	0.18	0.00	0.40	11.20	5.48	0.03	3.49

Table 2a: Trace element abundances in ppm within the low-Si type adakitic rocks.

(ppm)	Stan18A	Stan13A	Stan06B	Stan12A	Stan05C	Stan17A	Stan06A	Stan05A	Stan16C	Stan08A	Stan08B
Li	28	37	107	41	22	121	97	23	84	20	n.a.
Sc	25	8	13	21	10	12	12	11	9	6	n.a.
V	220	194	128	172	130	119	118	135	96	82	n.a.
Co	42	40	31	34	28	29	27	32	21	17	n.a.
Ni	92	100	27	50	20	32	25	21	19	11	n.a.
Cu	61	68	29	40	23	29	25	24	19	53	n.a.
Zn	118	99	128	96	98	103	95	130	118	118	90
Ga	16	14	17	17	18	17	17	19	17	16	16
Ge	1.088	1.037	0.885	0.076	1.074	0.904	0.959	1.15	0.075	0.764	n.a.
Rb	52	35	51	90	90	68	62	96	76	90	97
Sr	1804	2232	2355	1760	1207	2473	2347	1270	2112	1057	1068
Zr	172	139	214	212	211	220	217	226	238	211	228
Cs	12	3	8	58	3	1	12	3	2	1	n.a.
Ba	1904	2217	3361	2279	1852	2875	3052	2009	2765	3809	4156
Hf	3.636	3.163	3.852	4.232	4.17	4.039	3.972	4.335	4.279	3.757	n.a.
Pb	7.957	7.923	13.801	6.093	11.291	17.914	12.496	13.926	14.831	14.32	15.1
Th	9.735	7.606	16.868	9.748	16.223	19.126	17.796	16.5	20.535	19.842	23.4
U	2.248	2.193	4.168	2.144	3.621	4.866	4.477	3.925	5.153	5.442	5.9
La	95.647	101.241	171.92	114.357	114.775	166.569	167.482	116.057	157.788	147.568	n.a.
Ce	193.874	193.733	294.237	197.249	201.487	287.164	287.054	201.185	269.295	251.189	n.a.
Pr	20.91	19.841	29.462	21.338	19.546	28.502	28.189	19.905	25.901	24.39	n.a.
Nd	79.511	72.058	101.78	78.203	67.658	97.322	96.914	68.501	87.892	81.188	n.a.
Sm	11.684	10.054	13.824	11.489	9.424	13.266	13.158	9.569	11.556	10.728	n.a.
Eu	3.452	3.174	4.621	3.723	3.045	4.167	4.295	3.111	3.867	3.752	n.a.

Gd	8.261	6.836	10.019	9.663	6.928	9.377	9.069	7.008	8.06	7.177	n.a.
Tb	1.064	0.881	1.252	1.331	0.916	1.209	1.192	0.932	1.056	0.922	n.a.
Dy	5.044	4.041	5.995	7.056	4.637	5.549	5.62	4.645	5.003	4.267	n.a.
Ho	0.864	0.675	1.026	1.343	0.815	0.978	0.959	0.84	0.864	0.756	n.a.
Er	2.39	1.862	2.843	3.796	2.292	2.752	2.689	2.401	2.465	2.133	n.a.
Tm	0.302	0.225	0.361	0.497	0.31	0.346	0.341	0.318	0.317	0.276	n.a.
Yb	1.835	1.281	2.171	2.909	1.918	2.086	2.059	1.95	1.923	1.652	n.a.
Lu	0.274	0.182	0.323	0.445	0.292	0.315	0.308	0.298	0.293	0.25	n.a.
Y	25.351	19.053	29.599	54.226	24.27	28.312	28.093	24.816	25.794	22.464	24.7

Table 2b: Trace element abundances in ppm within the high-Si type adakitic rocks.

(ppm)	Stan01A	Stan19A	Stan20A	Stan13B	Stan02A	Stan09A	Stan11A	Stan10B	Stan09B	Stan10A
Li	20	n.a.	44	n.a.	n.a.	41	36	39	44	n.a.
Sc	0.924	n.a.	1.927	n.a.	n.a.	1.418	1.294	1.29	1.21	n.a.
V	8.954	n.a.	1.636	n.a.	n.a.	1.958	2.239	2.116	3.094	n.a.
Co	13.543	n.a.	1.4	n.a.	n.a.	8.968	7.373	5.799	15.899	n.a.
Ni	0.466	n.a.	0.065	n.a.	n.a.	0.112	0.225	0.45	0.226	n.a.
Cu	5.29	n.a.	2.909	n.a.	n.a.	8.069	5.473	11.227	4.293	n.a.
Zn	120	162	83	103	128	110	105	139	112	112
Ga	23	23	31	22	21	31	28	29	26	24
Ge	0.754	n.a.	1.217	n.a.	n.a.	0.032	0.017	0.007	0.02	n.a.
Rb	176	190	267	153	164	227	202	206	203	192
Sr	661	157	203		477	71	149	305	136	89
Zr	570	976	1018	500	615	953	820	859	736	749
Cs	2.807	n.a.	0.936	n.a.	n.a.	3.889	3.929	3.437	3.418	n.a.
Ba	540	272	9	527	667	161	216	274	291	249
Hf	8.789	n.a.	15.318	n.a.	n.a.	14.614	13.537	13.676	11.575	n.a.
Pb	24.377	24	30.209	25	27	22.77	25.221	26.268	23.132	24
Th	41.154	45	80.352	37	43	41.416	40.571	40.97	39.084	44
U	11.28	13	23.724	13	11	13.108	12.858	13.212	11.158	13
La	107.808	n.a.	133.796	n.a.	n.a.	65.999	86.092	87.489	109.919	n.a.
Ce	180.932	n.a.	212.182	n.a.	n.a.	113.997	145.686	146.756	183.441	n.a.
Pr	16.222	n.a.	16.868	n.a.	n.a.	10.483	12.859	12.905	16.07	n.a.
Nd	48.171	n.a.	46.044	n.a.	n.a.	29.914	37.374	37.522	47.516	n.a.
Sm	6.169	n.a.	5.663	n.a.	n.a.	3.978	4.812	4.765	5.867	n.a.
Eu	1.683	n.a.	0.874	n.a.	n.a.	0.943	1.148	1.135	1.382	n.a.

Gd	4.299	n.a.	3.978	n.a.	n.a.	2.864	3.423	3.325	4.103	n.a.
Tb	0.638	n.a.	0.623	n.a.	n.a.	0.455	0.543	0.517	0.603	n.a.
Dy	3.421	n.a.	3.512	n.a.	n.a.	2.743	2.992	2.919	3.298	n.a.
Ho	0.677	n.a.	0.726	n.a.	n.a.	0.561	0.606	0.591	0.63	n.a.
Er	2.165	n.a.	2.489	n.a.	n.a.	1.857	1.99	1.918	1.954	n.a.
Tm	0.34	n.a.	0.428	n.a.	n.a.	0.318	0.327	0.322	0.312	n.a.
Yb	2.308	n.a.	3.111	n.a.	n.a.	2.298	2.363	2.251	2.209	n.a.
Lu	0.367	n.a.	0.538	n.a.	n.a.	0.378	0.38	0.373	0.369	n.a.
Y	20.788	26	23.416	19	34	17.424	19.119	18.962	20.256	22

Table 3: Comparison between preferred values from GeoReM database (http://georem.mpch-mainz.gwdg.de/) for 3 USGS international standard reference materials (BCR-2, Columbia River Basalt; DNC-1, Braggtown NC. Olivine-normative dolerite; W-2, Centerville VA. Diabase) and our measurments.

(ppm)	ref BCR2	BCR-2	% recovery	ref DNC-1	DNC-1	% recovery	ref W-2	W2	% recovery
Li	9	9.364	-4	5.1	4.915	4	9.3	9.56	-3
Sc	33	34.942	-6	31	31.385	-1	35.9	37.378	-4
V	416	418.989	-1	148	136	8	268	256.964	4
Co	37	36.418	2	54.7	55.383	-1	45	44.123	2
Ni	12	11.596	3	256	260.03	-2	72	70.622	2
Cu	19	18.402	3	100	101.48	-1	105	117.459	-12
Zn	127	125.267	1	70	76.049	-9	77	72.998	5
Ga	23	22.842	1	15	14.339	4	18	18.75	-4
Ge	1.5	1.501	0	1.3	1.281	1	1.55	1.502	3
Rb	46.9	47.515	-1	3.9	3.399	13	21	20.291	3
Sr	340	339.691	0	144	138.424	4	196	197.908	-1
Zr	184	177.447	4	38	34.506	9	92	91.105	1
Cs	1.1	1.31	-19	0.21	0.22	-5	0.92	1.022	-11
Ba	677	641.206	5	103.3	99.777	3	172	167.183	3
Hf	4.8	4.583	5	1.01	0.918	9	2.45	2.395	2
Pb	11	11.103	-1	6.3	6.846	-9	7.7	8.151	-6
Th	5.7	5.342	6	0.24	0.238	1	2.17	2.107	3
U	1.69	1.561	8	0.06	0.056	6	0.51	0.5	2
La	24.9	24.832	0	3.53	3.666	-4	10.8	10.443	3
Ce	52.9	53.566	-1	8.11	8.087	0	23.4	22.85	2
Pr	6.7	6.82	-2	1.1	1.08	2	3	2.961	1
Nd	28.7	29.034	-1	4.86	4.964	-2	13	12.893	1

Sm	6.58	6.592	0	1.38	1.391	-1	3.3	3.206	3
Eu	1.96	1.989	-1	0.57	0.569	0	1.08	1.043	3
Gd	6.75	6.825	-1	2	2.062	-3	3.66	3.7	-1
Tb	1.07	1.065	0	0.39	0.387	1	0.62	0.607	2
Dy	6.41	6.646	-4	2.7	2.752	-2	3.79	3.831	-1
Ho	1.28	1.322	-3	0.62	0.614	1	0.79	0.775	2
Er	3.66	3.766	-3	1.87	1.882	-1	2.22	2.216	0
Tm	0.54	0.539	0	0.33	0.294	11	0.33	0.323	2
Yb	3.38	3.492	-3	1.97	1.896	4	2.05	2.029	1
Lu	0.503	0.523	-4	0.309	0.299	3	0.31	0.303	2
Y	37	37.18	0	17.7	17.786	0	22	21.798	1